

Development and Application of a Simplified Coplane Wind Retrieval Algorithm Using Dual-Beam Airborne Doppler Radar Observations for Tropical Cyclone Prediction

CHRISTOPHER MELHAUSER AND FUQING ZHANG

Department of Meteorology, and Center for Advanced Data Assimilation and Predictability Techniques, The Pennsylvania State University, University Park, Pennsylvania

(Manuscript received 11 September 2015, in final form 24 March 2016)

ABSTRACT

Based on established coplane methodology, a simplified three-dimensional wind retrieval algorithm is proposed to derive two-dimensional wind vectors from radial velocity observations by the tail Doppler radars on board the NOAA P3 hurricane reconnaissance aircraft. Validated against independent in situ flight-level and dropsonde observations before and after genesis of Hurricane Karl (2010), each component of the retrieved wind vectors near the aircraft track has an average error of approximately 1.5 m s^{-1} , which increases with the scanning angle and distance away from the aircraft track. Simulated radial velocities derived from a convection-permitting simulation of Karl are further used to systematically quantify errors of the simplified coplane algorithm. The accuracy of the algorithm is strongly dependent on the time between forward and backward radar scans and to a lesser extent, the zero vertical velocity assumption at large angles relative to a plane parallel with the aircraft wings. A proof-of-concept experiment assimilating the retrieved wind vectors with an ensemble Kalman filter shows improvements in track and intensity forecasts similar to assimilating radial velocity super observations or the horizontal wind vectors from the analysis retrievals provided by the Hurricane Research Division of NOAA. Future work is needed to systematically evaluate this simplified coplane algorithm with proper error characteristics for TC initialization and prediction through a large number of events to establish statistical significance.

1. Introduction

Recent studies demonstrate that ingestion of Doppler velocity observations from the tail Doppler radar (TDR) on board the NOAA P3 aircraft into convection-permitting hurricane prediction models can considerably improve tropical cyclone (TC) forecasts, especially the intensity (Zhang and Weng 2015; F. Zhang et al. 2011; Weng and Zhang 2012; Aksoy et al. 2010). Doppler velocity observations only provide information about the wind magnitude and direction along the radar beam, but the scanning strategy of the NOAA TDR can be exploited to derive the cross-beam component of the wind field. This additional cross-beam information is advantageous for improving forecasts when assimilated from land-based radars (Li et al. 2013; Wang et al. 2014) and airborne radars (Li et al. 2014).

The TDR is a conically scanning radar mounted on the tail of the NOAA P3 aircraft with a tilt angle $\theta_{\text{fore/aft}}$ of 20° from a plane normal to the flight track, scanning forward (fore) and backward (aft) using the fore/aft scanning technique (Frush et al. 1986; Hildebrand et al. 1986; Gamache et al. 1995). Since the aircraft is moving, each radar sweep traces out a helical pattern (Fig. 1a). A dual-Doppler analysis (Armijo 1969) can exploit the fore/aft scanning technique geometry, combining the mass continuity equation, a fall speed correction based on radar reflectivity, and multiple Doppler velocity observations interpolated to a common grid to derive a three-dimensional wind field.

Doppler velocity measurements from precipitation radars, such as the NOAA P3 TDR, are the horizontal and vertical motions of scatters (e.g., hydrometeors, insects, debris) in the wind field, not the actual air motions. The horizontal motions of the scatters are assumed to be comparable to that of the horizontal air motion, but the vertical motion of the scatters is a combination of the fall speed of the hydrometeors and the vertical air motion (Fig. 1c). Using the bulk estimate of the precipitation fall

Corresponding author address: Fuqing Zhang, Department of Meteorology, The Pennsylvania State University, University Park, PA 16802.
E-mail: fzhang@psu.edu

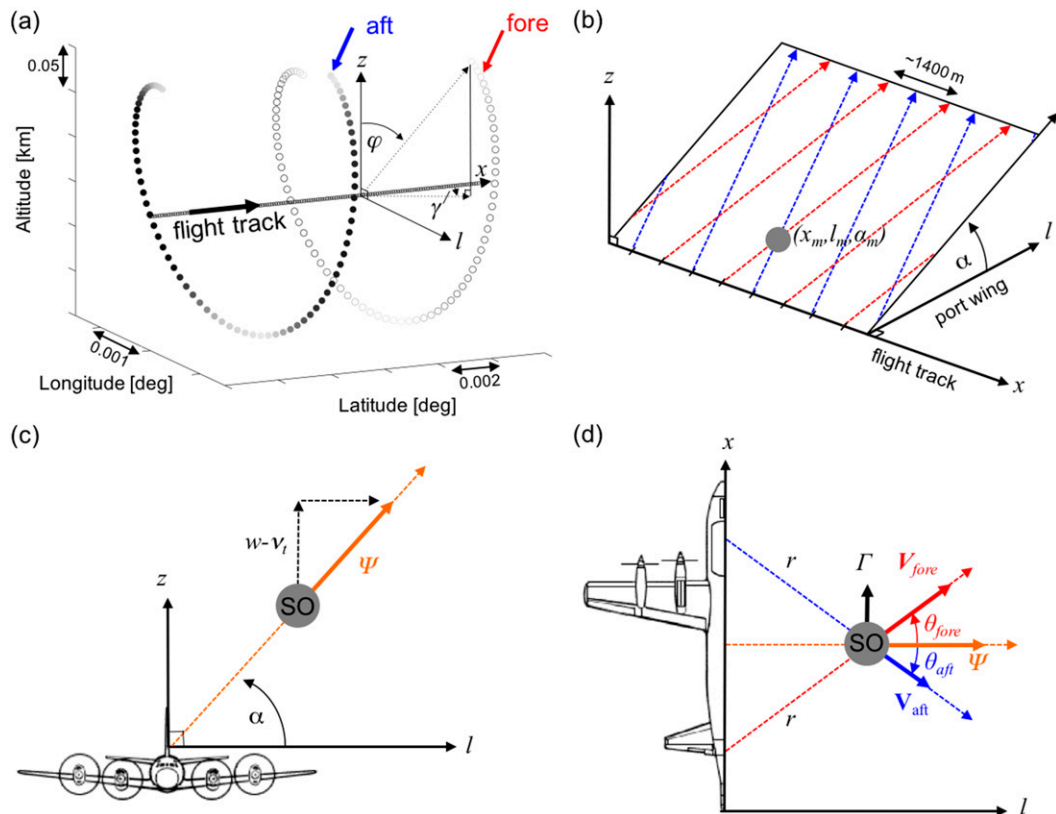


FIG. 1. Spatial configuration of a plane flying north for (a) a dual-beam airborne fore/aft scan of radial velocities at an arbitrary radial distance, each dot represents a simulated radial velocity; (b) the coplane-scanning geometry in natural cylindrical coordinates (x, l, α) ; (c) fall speed component of radial velocity along an arbitrary coplane point (x_m, l_m, α_m) ; and (d) retrieved wind components alongtrack Γ and perpendicular to track Ψ , geometrically derived from V_{fore} and V_{aft} with beam orientation (θ_{fore}, α) and (θ_{aft}, α) , respectively.

speed (Rogers 1964), a relationship between the reflectivity and height can be specified (e.g., Marks and Houze 1987) above, at, and below the melting layer to estimate bulk fall speeds for rain (Joss and Waldvogel 1970) and snow (Atlas et al. 1973; Gunn and Marshall 1958). This bulk vertical fall speed correction is applied to derive the true vertical air motion, introducing uncertainties in the retrieved vertical velocities.

Jorgensen et al. (1996) formulated the dual- and quad-Doppler retrieval methodology in Cartesian coordinates for the airborne TDR fore/aft scanning geometry. Their study quantified the three-dimensional error variance as a function of geometric viewing angle, taking into account uncertainties in the raw radial velocity estimates. There is additional error associated with raw airborne radial velocity measurements over ground-based measurements, stemming from the errors in the radar-pointing angles due to the aircraft motion (Jorgensen et al. 1983). The error variance for this mechanism was estimated to be approximately $0.7\text{--}1.1\text{ m s}^{-1}$, larger than the ground-based result of approximately

0.03 m s^{-1} . Combining radar-pointing angles and geometric viewing angle errors, the root-mean-squared error (RMSE) associated with the airborne TDR radial velocity observation is estimated as approximately 1.5 m s^{-1} (Jorgensen et al. 1996).

Although dual-Doppler analyses are routinely performed in Cartesian space (e.g., Frisch et al. 1974; Ray et al. 1975; Mohr et al. 1981), the geometry of the airborne fore/aft scanning technique is naturally expressed in cylindrical coordinates. A dual-Doppler analysis using the coplane scanning technique (Lhermitte and Miller 1970)—originally designed to be used with two ground-based radars—provides a natural extension of deriving a dual-Doppler analysis for the airborne TDR (Fig. 1b) in cylindrical coordinates. Chong and Testud (1996) applied the coplane scanning technique to airborne TDR velocity observations of a tropical squall line, demonstrating the advantages over traditional methods: not requiring an iterative process to solve for the wind field while mathematically describing a well-posed solution for determining the three-dimensional

wind field. Their study found that the coplane technique provides high-quality dual-Doppler wind estimation, but errors derived from boundary condition assumptions and the anelastic mass continuity equation constraint increases the uncertainty in the three-dimensional wind field retrieval, especially near the boundaries of the analysis. A recent study by [Didlake et al. \(2015\)](#) applied the coplane dual-Doppler wind retrieval technique to the NASA High-Altitude Wind and Rain Airborne Profiler (HIWRAP) dual-beam conically scanning, downward-pointing airborne radar. Errors for the coplane technique applied to the HIWRAP geometry for the along-aircraft track component, the cross-aircraft track component, and the derived vertical component were examined using a model-simulated TC and HIWRAP radar observations for Hurricane Ingrid (2013). This study showed a strong dependence of the errors in the retrieved three-dimensional wind field on the quality of the boundary conditions.

Early dual-Doppler analysis approaches interpolated radial velocities to a common grid and solve the dual-Doppler projection equations, using set boundary conditions and integrating mass continuity from the boundary throughout the analysis domain ([Bohne and Srivastava 1976](#); [Ray et al. 1980](#); [Marks and Houze 1984](#); [Didlake et al. 2015](#)). Another approach is to solve an optimization problem, minimizing a cost function that describes the misfit between the radial velocity observations and the radial velocity equation. This optimization problem can be a simple least squares approach or a variational approach including additional constraints such as mass continuity and boundary conditions to improve the three-dimensional wind field retrieval (e.g., [Ziegler 1978](#); [Chong and Campos 1996](#); [Gao et al. 1999](#); [Guimond et al. 2014](#)). The variational optimization approach bypasses the issue of integrating mass continuity and directly propagating boundary errors throughout the analysis domain, but substantial errors from the boundaries can still be propagated throughout the domain during the minimization process ([Gao et al. 1999](#)). This approach is used by the Hurricane Research Division (HRD) to produce the dual-Doppler radar TC analysis from the NOAA P3 TDR ([Gamache 1997](#)).

For TCs, it has been shown that the vertical wind component has a small correlation with other state variables ([Poterjoy and Zhang 2011](#)) with most of the information provided in the u - and v -wind field. Generally, the goal of any dual-Doppler analysis is to produce the lowest error estimate of the three-dimensional wind field. It is advantageous to assimilate vector wind observations into a model for TC prediction without potentially adding additional error by applying a mass continuity constraint.

This study will use the dual-Doppler projection equations formulated in cylindrical coordinates for the airborne fore/aft scanning TDR ([Chong and Testud 1996](#)) to estimate only the two-dimensional wind components, deriving errors associated with fall speed contamination and fore/aft scanning technique scan time differences with the simplification.

The authors wish to explore the use of the fore/aft scanning geometry and coplane technique without applying the mass-continuity equation to derive a low error wind estimate of the two-dimensional u - and v -wind field for the primary purpose of TC data assimilation and prediction. The questions motivating the study are (i) What are the temporal errors in the retrieved u - and v -wind field due to the time lag between fore/aft scans? (ii) What is the impact of the fall speed correction on the retrieved u - and v -wind field? (iii) How does the retrieved u - and v -wind field from the simplified coplane analysis compare to the variational HRD dual-Doppler analysis? (iv) What is the appropriate value of observational error for the u and v wind from this simplified coplane analysis for the purpose of data assimilation? (v) Can the simplified coplane analysis observations help improve TC track and intensity forecasts?

An overview of the simplified coplane methodology and simulated radial velocity methodology including model simulations used to generate a simulated TC u - and v -wind field are described in [section 2](#). [Section 3](#) presents the results comparing the simplified coplane analysis and the conventional HRD hurricane wind field analysis with in situ flight-level data and dropsondes, and [section 4](#) extends the comparison using simulated radial velocities for the simplified coplane analysis. [Section 5](#) describes forecast experiments assimilating simplified coplane analysis observations. Conclusions are given in [section 6](#).

2. Data and methodology

a. Case in study

Hurricane Karl (2010), which formed during the Pre-Depression Investigation of Cloud-Systems in the Tropics (PREDICT) experiment ([Montgomery et al. 2012](#)), the NASA's Genesis and Rapid Intensification Processes (GRIP) experiment ([Braun et al. 2013](#)), and the NOAA's Intensity Forecast Experiment (IFEX; [Rogers et al. 2006](#)) is used as a case study to test the simplified coplane u - and v -wind retrievals using the TDR radial velocity observations. Karl was the eleventh named storm of the 2010 Atlantic hurricane season becoming a TC at 1800 UTC 14 September 2010 before making first land-fall over the Yucatan Peninsula and moving into the Bay of Campeche the morning of 16 September 2010. Once

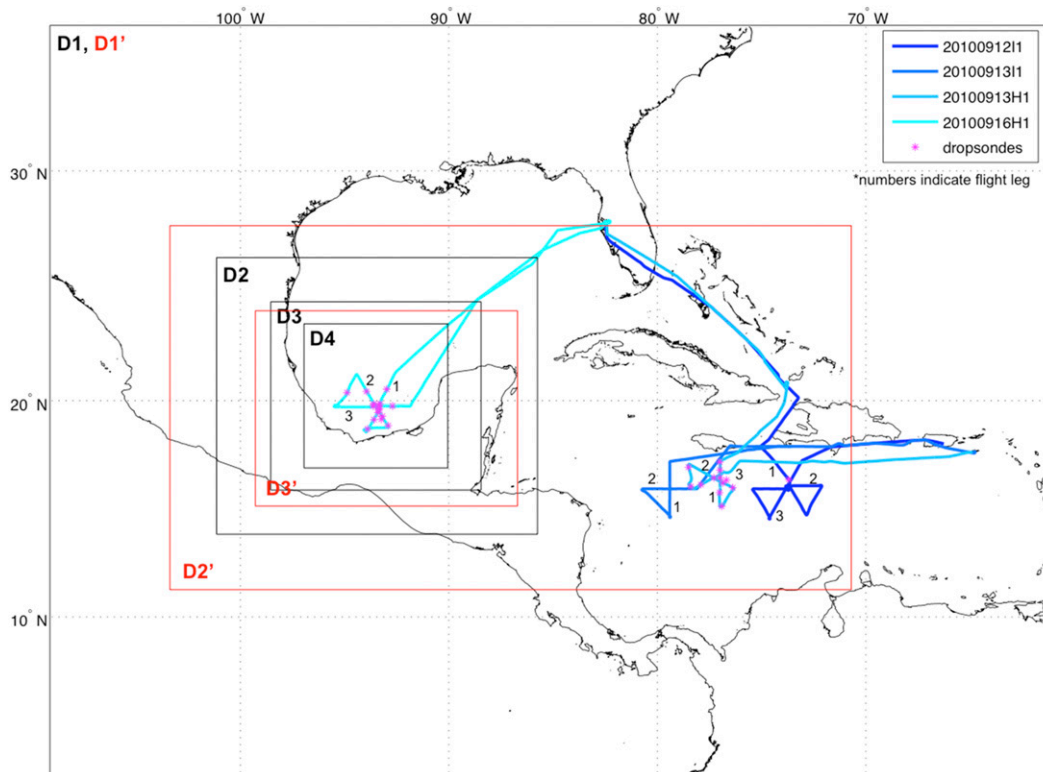


FIG. 2. Diagram of WRF domains used for the Hurricane Karl observing simulation experiment (black; D1–D4), WRF domains used for ensemble Kalman filter data assimilation experiments (red; D1'–D3'), NOAA P3 flights on 12 Sep 2010 (N-43; 20100912H1), 13 Sep 2010 (N-43; 20100913H1), 13 Sep 2010 (N-42; 20100913H1), and 16 Sep 2010 (N-43; 20100916H1) with numbered flight legs (blue shaded lines), and dropsondes used for coplane and HRD analysis validation (pink dots). Note: D1 and D1' are the same domains.

over the Bay of Campeche, it quickly intensified in the favorable high sea surface temperature and low vertical wind shear environment, intensifying into a category 3 hurricane on 17 September 2010, just prior to landfall in central Mexico. Both NOAA 42 and NOAA 43 P3 aircraft flew a total of four flights, each of which comprised two or three flight legs (Fig. 2). Three of the flights were during the pregenesis phase on 12 and 13 September 2010 and one was during the postgenesis phase just prior to rapid intensification on 16 September 2010. We will validate the simplified coplane observations of this study with flight-level measurements on board the NOAA P3 aircraft and dropsonde data from each NOAA P3 aircraft, the NOAA G-IV, and multiple PREDICT/GRIP aircraft platforms during Hurricane Karl (Fig. 2).

b. A brief review of the coplane geometry

A detailed derivation of the coplane methodology, including all assumptions and equations can be found in Chong and Testud (1996) (their section 2b). For this study, the coordinate convention of Chong and Testud

(1996) is used to describe the relevant geometry of the simplified coplane retrieval algorithm.

The fore/aft scanning technique generates radial velocities in a helical geometry around the flight track at each specified range gate—a single radial distance is diagramed in Fig. 1a. Assuming the aircraft track has minimal deviations in heading and altitude, a series of fore/aft radar beams can be structured into a half-plane about the flight track axis (Fig. 1b). A point on the half-plane can be described by (x_m, l_m, α_m) , where x is the distance along the flight track, l is the perpendicular distance from the flight track, α is the elevation angle of the tilted half-plane, and the m subscript corresponds to a single point. An angle $\alpha = 0^\circ$ describes the half-plane parallel to the earth's surface on the port side of the aircraft and monotonically increases in value clockwise. Focusing on a single intersection of the fore/aft beam on an arbitrary α plane (Fig. 1d), the distance of a radial bin along radar beam r from the aircrafts TDR and the tilt angle θ of the TDR (the departure of TDR antennae from perpendicular to the aircraft's track, positive is toward the nose) fore/aft radar beams

are important for defining the geometry of the coplane scanning technique.

The aircraft-relative alongtrack component Γ and perpendicular to track component Ψ (defined positive away from the aircraft track; Fig. 1d) wind components can be evaluated by geometrically combining two radial velocity wind vectors V_{fore} and V_{aft} (positive defined toward the radar) at an intersecting point (x_m, l_m, α_m) on an α plane. When the α plane deviates from parallel with the earth's surface, the fall speed of hydrometeors in the radar sampling volume must be accounted for in the Γ and Ψ components. The simplified methodology of this study differs from Chong and Testud (1996) since the fall speed is already accounted for in the raw radial velocities and is not explicitly accounted for in the Γ - and Ψ -wind calculation [Eq. (4) in Chong and Testud (1996)]. The retrieved Γ - and Ψ -wind components can subsequently be converted to aircraft and ground-relative Cartesian u - and v -wind components.

c. A simplified coplane algorithm for TC initialization

The retrieved wind field for the simplified coplane analysis in the manuscript is intended for TC initialization, thus, the radial velocity data are statistically thinned and quality controlled prior to the coplane retrieval and the vertical velocity is neglected. As previously discussed, the vertical velocity has small correlations with other state variables in TCs (Poterjoy and Zhang 2011). By their nature, radar radial velocity data have high spatial and temporal resolutions, generating more observations than can be efficiently ingested by current data assimilation systems. Generating superobservations [superobbing (SO)] can greatly reduce the number of observations by removing partially redundant observations while minimizing the information lost and reducing observation random and representativeness errors (Lorenc 1981; Purser et al. 2000; Weng and Zhang 2012). A thinning and quality control procedure is applied using similar quality control procedures as Weng and Zhang (2012) for radial velocity observations, generating radial velocity superobservations before applying the coplane algorithm to retrieve the u - and v -wind components.

Typical NOAA P3 flight parameters—aircraft ground speed of 115 m s^{-1} , radar altitude of 3 km, radar antenna speed of 10 rpm, and radar tilt angle of 20° —produce a spacing between consecutive fore scans along the x axis (Fig. 1b) of 1400 m. Based on the coplane geometry, the spacing between offset coplane observations along the x axis is 700 m and along the l axis is 1100 m. The temporal resolution is highly dependent on the distance from the aircraft track. The coplane observation closest to the aircraft on a given α plane (approximately 700 m) uses

fore/aft scan data that are 10 s apart, but this increases to approximately 360 s by 60 km. Prior to the statistical thinning of the radial velocity data, the flight radials are first quality controlled for noisy data, ground reflection, aliasing, corrected for aircraft velocity and attitude, and corrected for hydrometeor fall speeds by the HRD (Gamache 1997). The processed radial velocities are further quality controlled and statistically thinned before calculating the coplane observations using the following steps:

- (i) Flight-level data and HRD processed radials are aligned with flight databased on flight time and radar radial time.
- (ii) The aircraft-relative azimuth and elevation angle are used to calculate θ and α (Fig. 1b) for each radar beam, the location (x_m, l_m, α_m) of each radial bin is calculated on each α plane, and each radar beam is then binned by α angle using a user-specified bin width (Fig. 3b).
- (iii) The intersection of each fore/aft scan defines the center of each coplane α -plane bin with mean values of the intersecting radial bins radar geometry (α, θ) and radar beam flight data (latitude, longitude, altitude) used to define the center position (latitude, longitude, altitude) of the coplane observation.
- (iv) The radial velocities of the closest three radial bins on either side of the fore/aft beam crossing (Fig. 3a) and the closest α plane within the coplane α -plane bin width (Fig. 3b) are used for quality control and V_{fore} and V_{aft} selection. Within the group of fore/aft radial velocities, radial velocities are removed that are missing; have values less than 2 m s^{-1} , which are indistinguishable from radar noise or have values greater than the unambiguous radial velocity of the TDR (71 m s^{-1} ; both these constraints are in addition to the HRD real-time radar processing); and are greater than twice the standard deviation of the group. Subsequently, if the group has less than four fore/aft radial velocity values remaining, that coplane observation is discarded.
- (v) The Γ wind and Ψ wind are calculated using the median of the quality-controlled fore/aft radial velocities and rotated to ground-relative u - and v -wind components.
- (vi) All coplane observations with fore/aft radial velocity standard deviations twice the standard deviation of the radial velocities in each complete fore/aft radar sweep are removed.
- (vii) All coplane observations that occur during flight track changes of greater than 0.5° s^{-1} are removed.

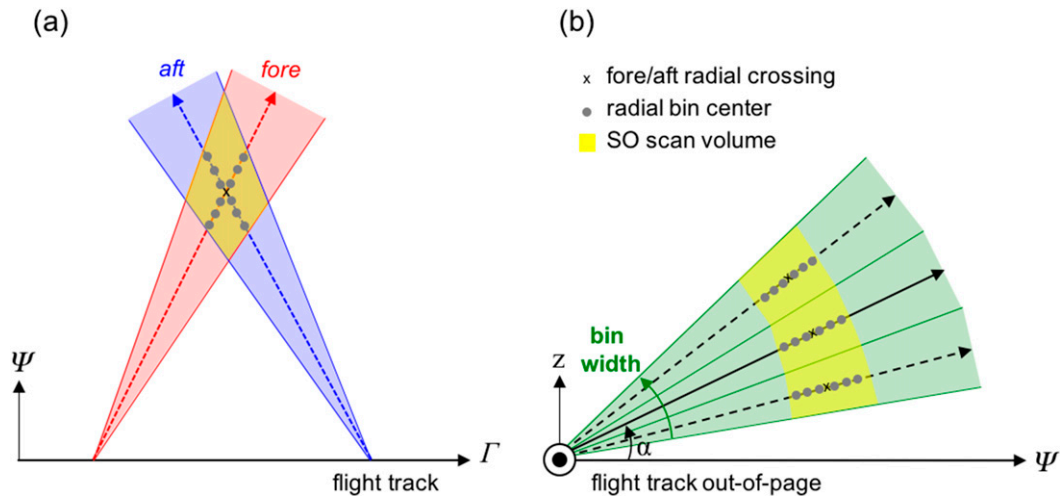


FIG. 3. Schematic of an arbitrary radial velocity fore/aft bin indicating the geometric center (black \times), the constituent fore/aft radial velocity observations (gray dots), and volume swept out by the coplane observation (yellow shading).

This simplified algorithm is used to generate coplane observations for both the simulated and the real NOAA P3 TDR data in this study. It should be noted that beam broadening has not been taken into account. Therefore, distances farther from the aircraft will represent a larger volume and thus representativeness errors will likely increase with increasing distance from the aircraft track, some of which may be partially mitigated by the radial velocity superobservation process.

d. Error analysis using a simulated tropical cyclone

1) MODEL SETUP AND INITIAL AND BOUNDARY CONDITIONS

The Advanced Research version of the Weather Research and Forecasting (WRF) Model (ARW), version 3.6 (Skamarock et al. 2008), is used to generate a convection-permitting simulation of Hurricane Karl and for the data assimilation experiments. Four two-way nested domains are used (Fig. 2) with horizontal grid spacing of 27 km (200×150 ; D1), 9 km (202×151 ; D2), 3 km (256×256 ; D3), and 1 km (430×430 ; D4), all with 61 vertical levels. Model physics include the WRF 6-class single-moment bulk microphysics scheme (Hong and Lim 2006), the modified Tiedtke cumulus parameterization (C. Zhang et al. 2011) for the coarse 27-km domain only, the Yonsei University planetary boundary layer scheme (Hong et al. 2006), the 5-layer thermal diffusion land surface model, and the Rapid Radiative Transfer Model shortwave and longwave radiation schemes (Iacono et al. 2008). The lack of cumulus parameterization in D2 will make little difference owing

to the two-way nesting; nearly all convective activity associated with Karl is within D3 and D4.

The initial and boundary conditions are generated from the Global Forecast System (GFS) Final (FNL) Analysis initialized at 1200 UTC 16 September 2010 with 6-h boundary tendency updates over the 36-h simulation duration. A 60-member ensemble is generated using the WRF Data Assimilation (WRFDA) System, version 3.6 (Barker et al. 2004), for assimilation of airborne radial velocity super observations at 1900, 2000, and 2100 UTC 16 September 2010 using the Pennsylvania State University (PSU) WRF ensemble Kalman filter (EnKF) system described in Zhang et al. (2009) and Weng and Zhang (2012). The use of airborne radial velocity superobservations helps constrain the vortex, simulating a more realistic, rapidly intensifying TC from 0000 to 1200 UTC 17 September 2010 compared with a simulation without data assimilation.

2) GENERATING SIMULATED RADIAL VELOCITIES

To simulate the NOAA P3 flight through the simulated TC, a three-leg butterfly-type pattern is flown using the high-resolution mean simulation for D4 starting at 1200 UTC 17 September 2010. The data are updated every 5 min during the simulated flight to account for storm evolution. The simulated aircraft is flown at 115 m s^{-1} at an altitude of 3000 m, similar to typical NOAA P3 aircraft flights. For simplicity, the attitude parameters (roll, pitch, and drift) are assumed to be 0° and the track angle is adjusted for each flight leg heading to generate the simulated butterfly legs.

The simulated TDR uses fore/aft scanning with a tilt angle ($\theta_{\text{fore}} = \theta_{\text{aft}}$; Fig. 1d) of 20° , a rotation rate of 10° s^{-1} with an azimuthal resolution of 0.75° , and a radial gate-to-gate resolution of 150 m, all typical parameters of the operational NOAA P3 TDR. The aircraft-relative azimuth and elevation angles of each radial beam are projected into ground-relative coordinates of radar azimuth and elevation angle; the standardized methodology is documented in Lee et al. (1994). Each radial bin position is corrected for refraction and the earth's curvature by applying a standard factor of 4/3 when calculating the radial bin height from the radar.

Using the aircraft position within the simulated ground-relative domain and ground-relative radial beam azimuth γ and elevation ϕ angles, the position of each radial bin is computed and radial velocity v_r calculated as

$$v_r = (\sin\gamma \cos\phi)u + (\cos\gamma \cos\phi)v + (\sin\phi)(w - v_t), \quad (1)$$

where u , v , and w are the model winds and v_t is the model derived fall speed correction linearly interpolated to the radial bin location. To simulate realistic airborne radial velocities, the model simulated reflectivity (Stoelinga 2005) is calculated at each model grid point, linearly interpolated to the radial bin location, and used to filter out any radial bins with a simulated reflectivity less than 15 dBZ. The model-simulated reflectivity is calculated and linearly interpolated to the radial bin location to compute the mean terminal fall speed of the hydrometeors using the fall speed correction described by Marks and Houze (1987). The algorithm is used on the modeled data to estimate the hydrometeor fall speed instead of the diagnostic fall speed calculated in the model microphysics scheme to keep consistency with the processing of the real-time and modeled data.

e. Testing the impact of the simplified coplane analysis observations on forecast track and intensity: Data assimilation methodology, model setup, and initial and boundary conditions

The WRF Model configuration including model physics and dynamics are the same as those used for the error analysis of the simulated TC, but the three two-way nested domains (Fig. 2) are slightly modified using only horizontal grid spacings of 27 km (200×150 ; D1'), 9 km (202×151 ; D2'), and 3 km (256×256 ; D3') with 43 vertical levels.

The initialization, boundary conditions, and data assimilation procedure is the same as those used for the error analysis of the simulated TC, except the experiments are initialized at 0000 UTC 16 September 2010 and the National Hurricane Center (NHC) best track position and intensity data are assimilated every

6 h to constrain the 60-member ensemble until the airborne observation assimilation beginning at 1900 UTC 16 September 2010.

3. Simplified coplane analysis: Flight-level and dropsonde error analysis

The horizontal and vertical spatial coverage of the simplified coplane observations are highly dependent on the quality of the fore/aft radial velocity observations. Any violation of the simplified coplane algorithm assumptions or data outside of specific thresholds discussed in section 2a will result in a degradation of quality (e.g., unrepresentative radial velocities contaminating the radial velocities) or complete removal of the retrieved winds since the minimum number of observations in the fore/aft bin are not met. Comparing the flight-level horizontal coverage of retrieved winds from the NOAA P3 flight leg 2 on 16 September 2010 between the simplified coplane analysis (Fig. 4a) and the HRD analysis (Fig. 4b), a reduction in coplane observation coverage is evident at large distances perpendicular to the flight track and locations of large flight track heading changes—particularly in the eye. The HRD analysis inherently smoothes the retrieved winds due to the variational technique used in its generation, thus small-scale details are removed. This is evidenced by the lack of detail in the wind speed, especially in the asymmetric maximum in wind speed in the northeast quadrant of Karl. This smoothing effect was discussed in Didlake et al. (2015) in terms of their global solver. The radial velocity superobservations of Weng and Zhang (2012) have a more complete spatial coverage (Fig. 4c) compared with that of the simplified coplane analysis due to the stricter quality control constraints on flight track and the need of both a fore/aft scan at each coplane observation location for the simplified coplane analysis.

a. Flight-level winds validation

The NOAA P3 aircraft have onboard instrumentation to provide in situ measurements of flight-level winds; useful to compare with retrieved u - and v -wind components closest to the aircraft track. The 10-s flight-level aircraft in situ u - and v -wind observation with the smallest temporal deviation from each coplane and HRD observation and falls within 2 km of the flight track are compared, effectively thinning the flight-level data to the simplified coplane analysis data. Each in situ measurement is used only once on each α plane. Flight-level wind comparison with retrieved wind components for pregenesis flight leg 2 on 13 September 2010 (Fig. 5) and postgenesis flight leg 2 on 16 September 2010 (Fig. 6) indicate strong agreement between both airplane-relative

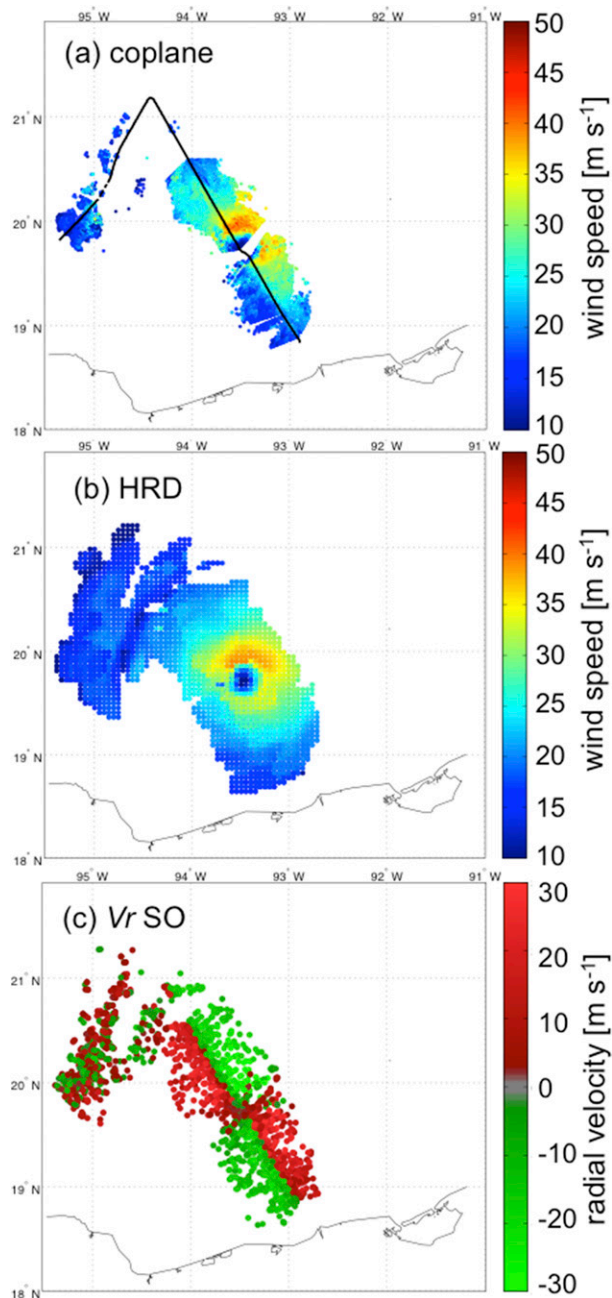


FIG. 4. Wind speed retrievals from the (a) simplified coplane analysis and (b) HRD analysis, and (c) radial velocity super-observations from flight leg 2 of the 16 Sep 2010 (N-42) mission.

(Γ and Ψ) and ground-relative (u and v) winds for the α planes parallel to the earth's surface ($\alpha = 0^\circ, 180^\circ$) and the HRD analysis. For the second leg of the flight on 13 September and 16 September 2010 (heading of approximately 315° ; Fig. 2), a slight bias of approximately 0.5 m s^{-1} exists in the Ψ wind for both pre- and post-genesis flights, which translates into both u - and v -wind components when rotated. The bias is a result of the

airplane heading departure from the track due to the southwest then northeast winds as the plane traverses the TC. This results in an overestimate of the observed winds when the radar beam is corrected for aircraft attitude. The sign of the bias depends on the α plane and increases in magnitude, up to 1 m s^{-1} for stronger circulations on 16 September 2010 compared with the earlier flights on 12 and 13 September 2010. Chong and Testud (1996) showed random errors in aircraft attitude parameters (pitch, roll, and drift) and systematic deviations to the aircraft track can increase errors in the coplane dual-Doppler analysis horizontal winds by as much as 0.5 m s^{-1} .

Focusing on the u - and v -wind components, Table 1 (top) provides the mean error (ME), mean absolute error (MAE), and RMSE statistics for each full flight and combined flights for the simplified coplane analysis; the same statistics for the HRD analysis are presented in Table 1 (bottom). The ground-relative wind component ME of all flights for both the coplane and the HRD analyses have a minimal bias and are generally consistent among all flights. The RMSE is generally smaller for the coplane observations compared with the HRD for individual flights and is $0.15\text{--}0.25 \text{ m s}^{-1}$ smaller on average for all NOAA P3 flights into Karl. Given the small bias, a larger variance is present in errors for the HRD-retrieved wind components compared to the simplified coplane analysis. It is more accurate compared to the HRD analysis when retrieving the u - and v -wind components closest to the aircraft. Reasor et al. (2009) presented a flight-level error analysis between 10 flight passes over the TC inner core of Hurricane Guillermo (1997) and an airborne dual-Doppler analysis following Gamache (1997), the same base method used in the HRD analysis. The bias of the HRD method in Table 1 is consistent between studies, although the RMSE of the current study is approximately $1\text{--}2 \text{ m s}^{-1}$ less, a substantial improvement. These results elucidate the benefits of the simplified coplane algorithm.

As the α plane deviates from parallel with the earth's surface, a vertical component is introduced into the Ψ -wind component and will contaminate the rotated ground-relative u - and v -wind components. An analytical derivation of this geometric error was described in Jorgensen et al. (1996) and corresponds well with the flight-level results. The Ψ wind is a function of the inverse cosine, thus increasing α will reduce the observed along-beam component, underestimating the ground-relative u - and v -wind components. Comparing the flight-level winds to the coplane u - and v -wind observations closest to the flight track while varying the α plane (Flight Level; Fig. 7) shows a large increase in RMSE that is observed as the radar beam attains a larger vertical component, an

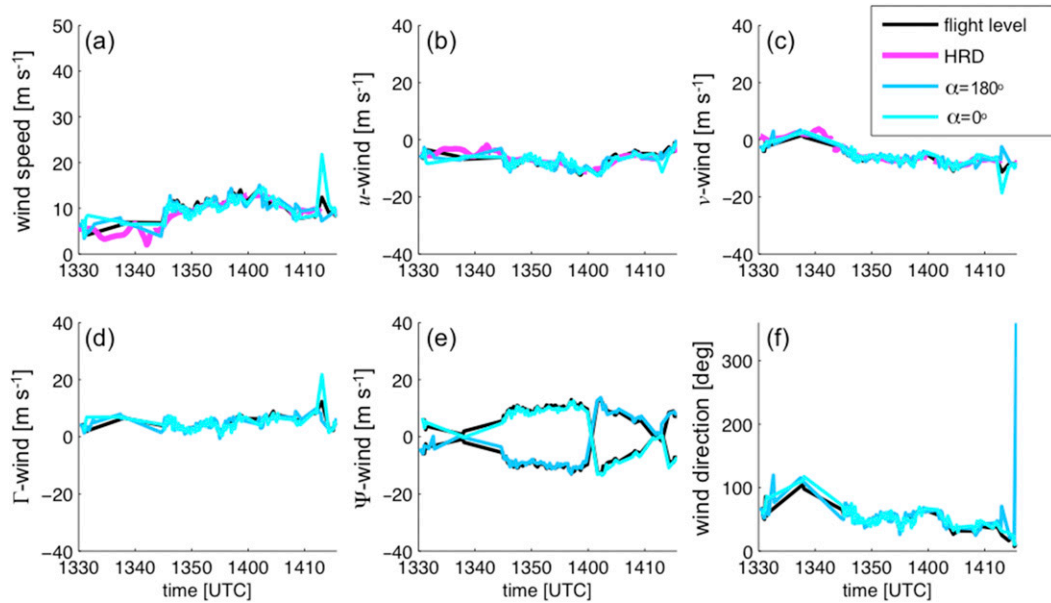


FIG. 5. Flight-level comparison of closest coplane observations to the flight track (<2000 m) on α plane 0° , 180° (blue colored lines), HRD analysis wind speeds closest to flight level (~ 3 km) and flight track (magenta line), and flight-level values (black line) from the aircraft of (a) wind speed, (b) u wind, (c) v wind, (d) Γ wind, (e) Ψ wind, and (f) wind direction from flight leg 2 of the 13 Sep 2010 (N-42) mission.

expected result. The lowest error retrievals are at small α -plane deviations, quickly exceeding 5 m s^{-1} by $\pm 50^\circ$ α -plane deviation; Jorgensen et al. (1996) recommended using observations within $\pm 45^\circ$.

b. Dropsonde validation

During each flight, the NOAA P3 aircrafts drop multiple dropsondes, an in situ instrument that can be used to validate radar retrievals below flight level far from the aircraft (Fig. 2). Also, aircraft from the GRIP and PREDICT field experiments, flying at higher altitudes, have dropsondes during each NOAA P3 flight that can be used to validate coplane observations at higher altitudes. In general, the RMSE for the simplified coplane-analysis-retrieved winds are smaller closer to the aircraft track and for smaller α -plane deviations from 0° and 180° , but no clear trend in errors exists for coplane observations retrieved farther from the aircraft (Fig. 7). When calculating errors between the coplane observations and each dropsonde observation, all dropsonde observations are smoothed and less than 2 km away from a specific coplane observation—by design—with a majority between 1 and 1.5 km (Fig. 8a). Because of the limited availability of dropsonde for comparison, the maximum perpendicular distance of observations from the aircraft is 22 km, only approximately 1/3 the distance the coplane algorithm assumptions allow. The increase in RMSE for coplane observations retrieved far from the aircraft

due to the fore/aft time delay assumption cannot be validated with this data source.

The dropsonde comparison errors for the simplified coplane analysis u - and v -wind components are normally distributed (Figs. 8b,c), with a general positive bias in the u - and v -wind [Table 2 (top)] components. Calculating errors using the same dropsonde observations for both the simplified coplane analysis [Table 2 (top)], and the HRD analysis [Table 2 (bottom)], the HRD analysis has a smaller RMSE for the u wind, but similar v -wind component. The HRD error results of approximately $2\text{--}3 \text{ m s}^{-1}$ are in agreement with a synthetic data study by Lorusolo et al. (2013) who found less than 2 m s^{-1} RMSE for the tangential wind not including errors introduced by aircraft attitude. Given the disparity in u - and v -wind dropsonde error statistics for both methods, a future study with more cases will need to be performed to better ascertain accurate dropsonde results. The statistics presented herein should be interpreted as a general estimate of approximately $1.5\text{--}2.75 \text{ m s}^{-1}$ error in either component.

4. Error analysis of the coplane algorithm through simulated NOAA P3 TDR data

The spatial deficiency in flight-level and dropsonde observations used for validation can be supplemented by simulating a NOAA P3 flight and radar data from an NWP simulation of a TC. The simulated radial

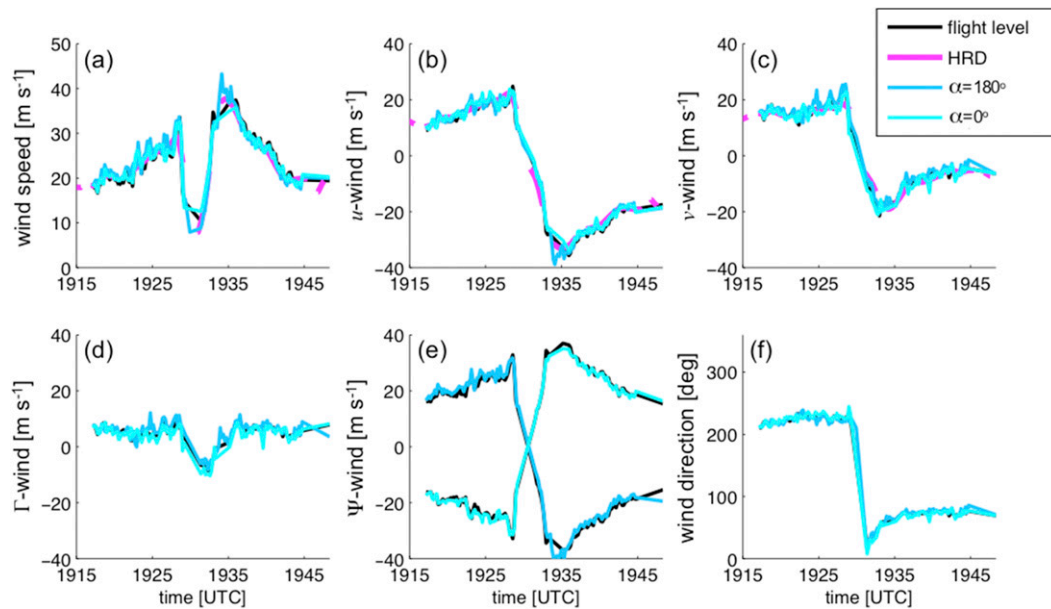


FIG. 6. As in Fig. 5, but from flight leg 2 of the 16 Sep 2010 (N-42) mission.

velocities are processed using the simplified coplane algorithm, retrieving the u - and v -wind components and compared with the true values at each coplane observation location interpolated from the true model simulation used to generate the simulated radials. The errors calculated using the simulated coplane observations do not include errors introduced by aircraft attitude, radar-pointing angle, or beam broadening, but provide an estimate of the fall speed assumption and temporal fore/aft timing assumption errors associated with the simplified coplane algorithm.

The simulated radial velocities are generated along three legs of a typical butterfly pattern flown by the NOAA P3 aircraft through a mature TC (Fig. 9a). The

flight track is ground relative, following a fixed path relative to the earth. The intersection of the three legs is the mean location of the eye during the simulated flight. The WRF simulation of Karl generates a realistic structure of the rapidly intensifying TC, albeit the simulation has a slightly weaker maximum 10-m wind speed and slightly higher minimum sea level pressure than the NHC best track data. The wind speed and u - and v -wind components at the beginning of the simulated radial velocity period for leg 1 at 0000 UTC 17 September 2010 (Figs. 9b–d) indicate a relatively small eye and mean circulation, both observed with Karl. A spatially similar spiral band structure for the observed storm is present in the simulated radar reflectivity field (Fig. 9a); the

TABLE 1. Individual and combined flight-level mean error (ME), mean absolute error (MAE), and root-mean-squared error (RMSE) of the retrieved u - and v -wind components of the (top) simplified coplane analysis and (bottom) HRD analysis compared with NOAA P3 flight-level winds. All values are in m s^{-1} .

	u wind			v wind		
	ME	MAE	RMSE	ME	MAE	RMSE
Flight-level simplified coplane analysis						
12 Sep 2010 (N-43)	0.13	1.25	1.71	−0.63	1.07	1.39
13 Sep 2010 (N-43)	−1.18	1.42	1.71	−0.07	0.48	0.57
13 Sep 2010 (N-42)	−0.03	0.93	1.27	0.00	0.92	1.26
16 Sep 2010 (N-42)	−0.01	1.35	1.81	−0.09	1.24	1.66
All flights	−0.05	1.22	1.66	−0.13	1.09	1.49
Flight-level HRD analysis						
12 Sep 2010 (N-43)	0.65	1.09	1.34	−0.33	1.00	1.26
13 Sep 2010 (N-43)	−0.75	2.12	2.47	−0.08	0.96	1.29
13 Sep 2010 (N-42)	0.16	1.40	1.73	−0.09	1.15	1.47
16 Sep 2010 (N-42)	0.18	1.58	2.13	−0.31	1.56	2.02
All flights	0.18	1.47	1.89	−0.20	1.25	1.65

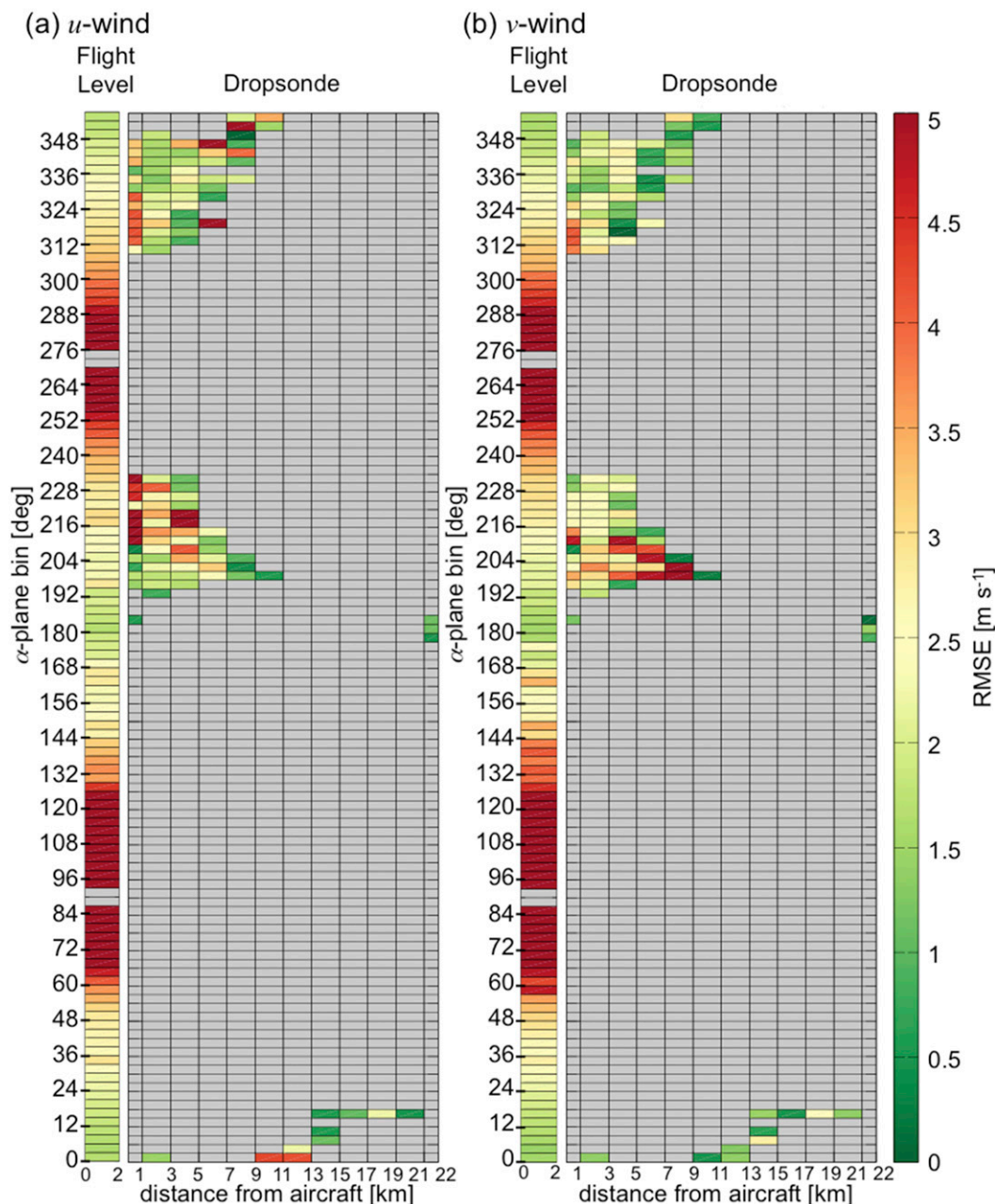


FIG. 7. Root-mean-squared error binned by α -plane bin and distance from flight track for (a) u wind and (b) v wind. “Flight Level” indicates wind component comparison of closest coplane observations to the flight track (<2000 m) for all available NOAA P3 flights [12 Sep 2010 (N-43), 13 Sep 2010 (N-43), 13 Sep 2010 (N-42), and 16 Sep 2010 (N-43)] and dropsonde indicates comparison of closest coplane observations to the available dropsonde observations for all available NOAA P3 flights and GRIP/PREDICT missions.

similarity is most notable in the southwest quadrant. Examining the simplified coplane analysis of the u - and v -wind components from the simulated radial velocities of leg 1 for the 0° and 180° α planes (Figs. 10a,b), the algorithm successfully retrieves an approximately homogenous and spatially dense set of observations. The retrieved u - and v -wind components have a similar

spatial pattern as the retrieved simulated reflectivity (Fig. 10c) used to filter out nonrepresentative low dBZ retrievals. The simplified algorithm correctly captures the clear eye and breaks in between spiral bands in the southeast quadrant.

The errors in the simulated u - and v -wind components can be broken into four primary sources, stemming from

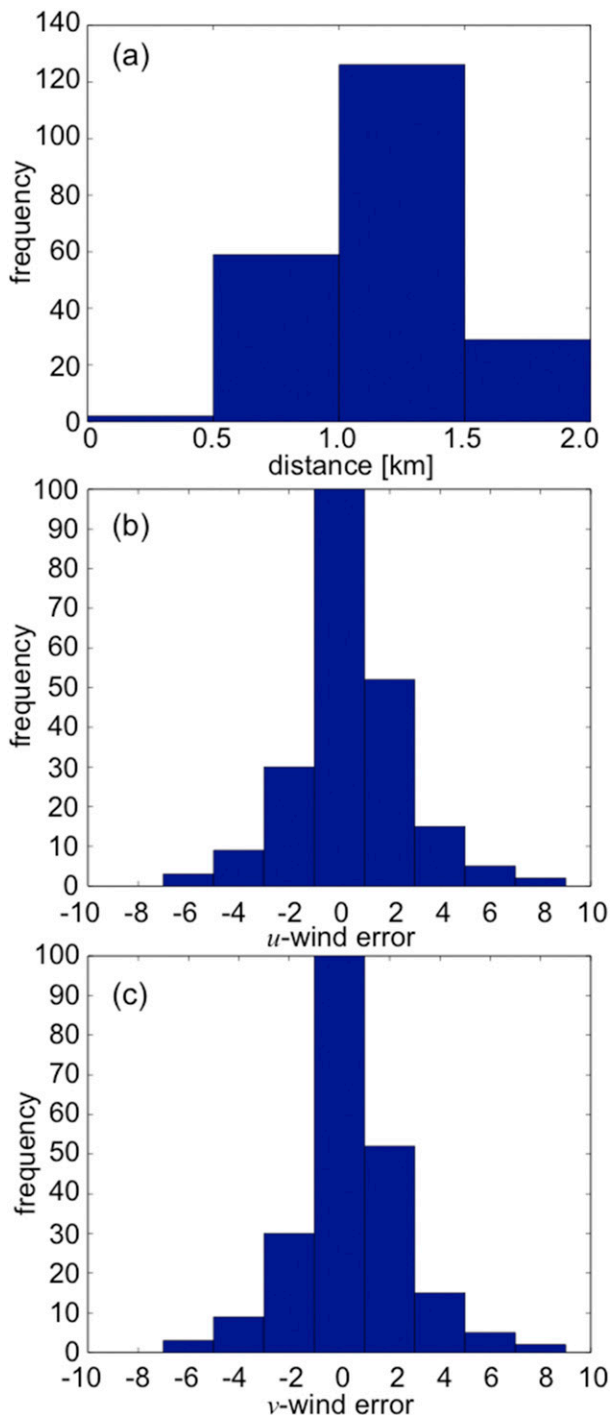


FIG. 8. Distributions of (a) distance between dropsonde observations and coplane observations, (b) u -wind errors, and (c) v -wind errors used to calculate dropsonde comparison statistics.

(i) the geometric errors of the coplane methodology, (ii) the radial velocity superobservation process, (iii) introduction of fall speed corrections, and (iv) the temporal assumptions associated with the use of fore/aft

scans at different times. Note that the temporal fore/aft scan error is not a surprising result, but has never been explicitly quantified in previous studies. Interpolation errors introduced from the discrete simulation grid are assumed small due to the high horizontal and vertical spatial resolution of the simulation. The analytical geometric errors for airborne dual-Doppler radar retrievals have been thoroughly documented by Jorgensen et al. (1996), the real data errors in this study closely match the documented analytical results. The radial velocity superobservation process may generate a representativeness error due to the use of a median fore/aft radial velocity to describe a radar volume that spans 18 fore/aft range gates (Figs. 3a,b). The two median values are then used to derive the Γ and Ψ wind. For this study, this source of error is not separated from the other three errors. The remainder of this section examines the fall speed and temporal assumption errors.

The spatial distribution of errors for the 0° and 180° α planes—these α planes minimize the contribution of errors due to fall speed contamination—exhibit the spatial error distribution expected from the temporal fore/aft assumption used in the coplane algorithm (Figs. 10d,e). Errors increase with increasing perpendicular distance from the aircraft track, a result of temporal representativeness error using aft radials valid further in the relative future compared with the fore scans valid time. It should be noted that since the simulated wind field is updated every 5 min with new simulation data fed to the coplane algorithm, artificial dislocation errors are present due to storm motion. The errors are exacerbated near regions with large gradients in wind speed.

The coplane geometry fully resolves winds parallel to the aircraft track although winds perpendicular to the track have a vertical component. Even though the coplane observations depicted in Fig. 10 are on horizontal α planes, each coplane observation is a binning of the closest radials within $\pm 1.5^\circ$ of the specified α planes. The radial velocity superobservation process implicitly introduces a vertical component for the horizontal planes. For flight leg 1, the largest errors in the u wind (Fig. 10d) fall to the left side of the aircraft heading and to the right side for the v wind (Fig. 10e) due to the backing from a predominantly easterly to northerly wind on the right side and flipping from an east-southeasterly to a west-southwesterly wind on the left side of the simulated aircraft. Because of the track heading, the simulated aircraft track has many more observations with large Ψ -wind components, manifested as larger errors on the right side of the plane heading when on the northern side and left side of the track when

TABLE 2. Individual and combined dropsonde mean error (ME), mean absolute error (MAE), and root-mean-squared error (RMSE) of the retrieved u - and v -wind components of (top) the simplified coplane analysis and (bottom) HRD analysis compared with available dropsondes from NOAA P3 flights, GRIP, and PREDICT missions. All values are in m s^{-1} .

	u wind			v wind		
	ME	MAE	RMSE	ME	MAE	RMSE
Dropsonde simplified coplane analysis						
13 Sep 2010 (N-42)	0.44	1.63	2.22	0.62	1.52	2.02
16 Sep 2010 (N-42)	1.06	2.01	2.98	-0.21	2.11	2.80
All flights	0.84	1.88	2.74	0.08	1.91	2.55
Dropsonde HRD analysis						
13 Sep 2010 (N-42)	-0.26	1.24	1.68	-0.10	1.01	1.29
16 Sep 2010 (N-42)	0.20	1.51	2.12	-0.53	2.01	2.97
All flights	0.05	1.42	1.98	-0.39	1.68	2.55

on the southern side of the simulated eye in the retrieved u - and v -wind fields.

The coplane observations presented in Fig. 10 use simulated radials that include the HRD fall speed correction. The higher fall speeds v_r (Fig. 10e) for each coplane observation correspond to higher simulated maximum reflectivity (Fig. 10c) values, but given the small α -plane deviations, this only contributes to a small portion of the error in the u - and v -wind components for low α -plane deviation. Based on the simple geometry of the coplane algorithm, as the α -plane deviation increases from horizontal, the impact of vertical velocities becomes larger in the retrieved winds. Since the purpose of this study is for TC data assimilation purposes, the focus is how the fall speed correction error propagates into the components. Three additional experiments using temporally updated model fields were performed to isolate the impact of fall speed correction on the u - and v -wind components: assuming no vertical velocity (EXP_NOW), using the model vertical velocity (EXP_PERW), and subtracting the simulated HRD fall speed (EXP_FALL). The EXP_NOW simulation errors are a result of interpolation and the temporal disparity between fore/aft scans. Examining the impact of perpendicular distance from aircraft track by aggregating all α planes for all simulated flight legs (Fig. 11a), EXP_NOW has the lowest error of the temporal simulations, minimizing close to the aircraft track around 0.5 m s^{-1} and increasing to 1.75 m s^{-1} by 40 km where the largest disparity in timing arises.

Adding in the vertical motion in both EXP_PERW and EXP_FALL increases the RMSE over 1 m s^{-1} at all range bins, with the coplane observations within 10 km and large α -plane deviations dominating the error statistics. A drastic increase in RMSE is observed closest to the aircraft, a direct result of the coplane geometry. At larger α -plane deviations, the vertical velocity dominates the radial velocities, but is not retrieved by the

coplane algorithm; the w wind is assumed to be null and the v -wind error increases by $\cos^{-1}\alpha$. As the range increases from 10 km, valid quality-controlled radial velocities are constrained at smaller α -plane deviations and the errors associated with the null vertical velocity assumption in the coplane algorithm become irrelevant. An additional experiment keeping the fall speed correction, but holding the model fields static at the initial simulation time when retrieving the radial velocities (EXP_FALL_S) isolates the temporal disparity errors, reducing the errors by $2\text{--}3 \text{ m s}^{-1}$ at all perpendicular distances from the aircraft.

Examining the combined errors of the u - and v -wind coplane observations by α -plane bins (Fig. 11b) also exposes the high error dependence on the α -plane deviation. Below an α -plane deviation of $\pm 40^\circ$, the fore/aft temporal disparity is the primary contributor to the error, but the exclusion of the vertical velocity dominates at larger α -plane deviations. The local maxima in all temporal simulations (EXP_NOW, EXP_PERW, EXP_FALL) is close to α planes parallel to the earth's surface and arises from the increased perpendicular distance from the aircraft, thus an increased time between fore/aft scans. As expected, EXP_FALL_S minimizes at these angles. Breaking apart the EXP_FALL errors by bin and range for the u wind (Fig. 12a) and v wind (Fig. 12b) over all simulated legs, the aforementioned patterns of increasing error by α -plane deviation and perpendicular distance emerges. Strong regional fluctuations in the RMSE appear in the u - and v -wind error, an artifact of the limited grid spacing impacting the interpolation of model variables and the α -plane binning process.

The RMSEs for the u - and v -wind components (Table 3) of all simulated flight legs quantify the general error associated with the simplified coplane retrieval. The retrievals closest to the simulated aircraft at α planes of 0° and 180° at flight level have small errors

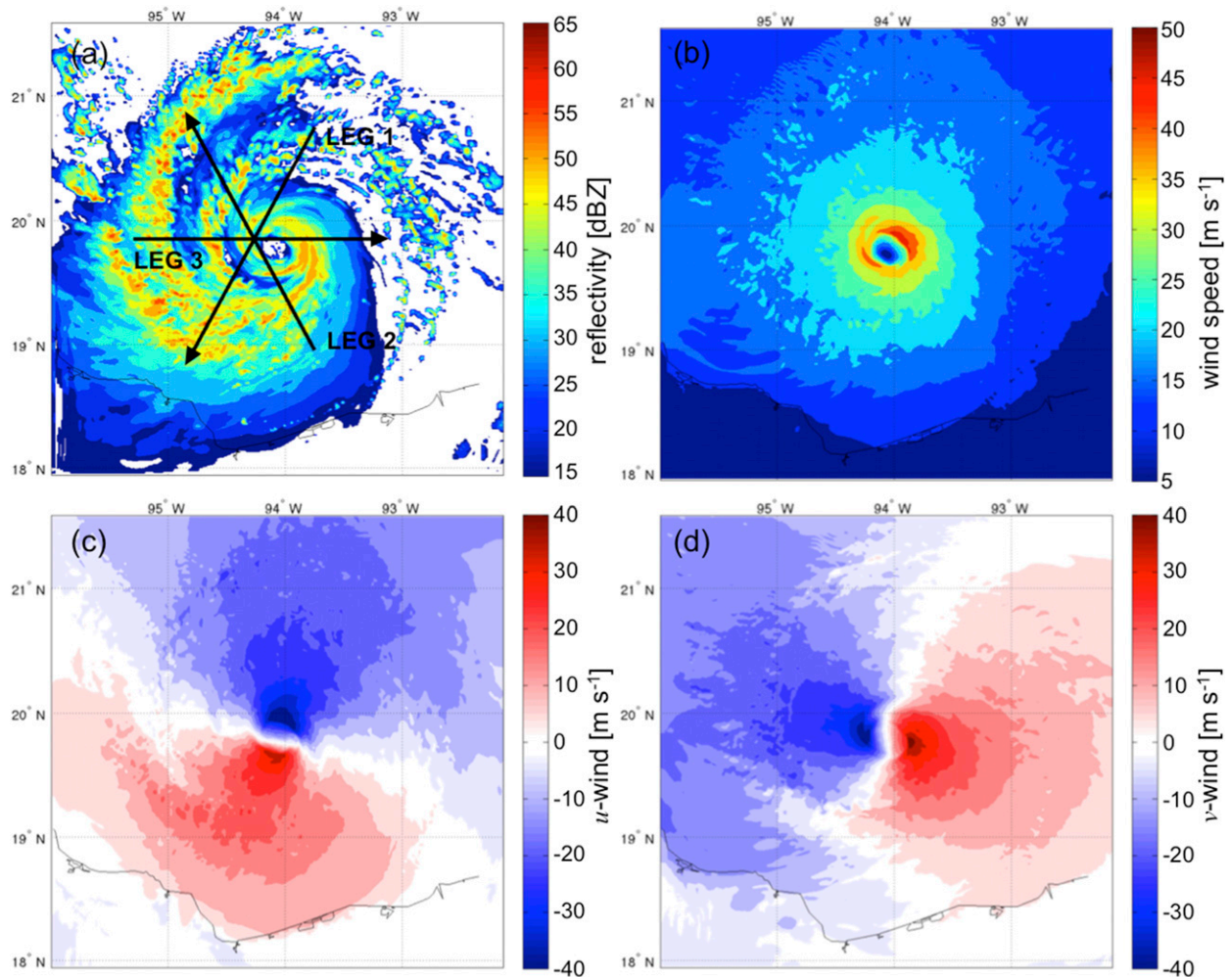


FIG. 9. WRF-simulated fields of (a) maximum radar reflectivity, (b) 10-m wind speed, (c) 10-m u wind, and (d) 10-m v wind at 0000 UTC 17 Sep 2010. The black arrows in (a) indicate the flight track legs used to simulate coplane observations.

of approximately $0.02\text{--}0.2\text{ m s}^{-1}$, predominantly interpolation errors. Extending to all coplane observations out to 40 km, the errors jump to approximately $2.2\text{--}2.3\text{ m s}^{-1}$, driven by the inclusion of the temporal fore/aft disparity assumption. Extending to α -plane deviations of $\pm 50^\circ$ and introducing the impacts of vertical motion minimally increases the RMSE, approximately 0.1 m s^{-1} . Restricting the perpendicular distance from the aircraft while maintaining the $\pm 50^\circ$ α -plane deviations slightly decreases the RMSE by approximately 0.1 m s^{-1} .

5. Impact of assimilating coplane observations on track and intensity forecasts

The simplified coplane analysis only uses geometry and does not require iterative algorithms or minimization techniques to derive the wind vectors, thus uses minimal

computing to generate low uncertainty u - and v -wind retrievals from the airborne TDR. Additionally, it does not require a full flight of radar data to generate the analysis and therefore can be more suitable for real-time applications. To demonstrate the viability of these observations for TC prediction, a proof-of-concept data assimilation experiment using airborne NOAA P3 TDR data of Karl between 1900 and 2100 UTC 16 September 2010 is performed. Seven experiments initialized at 0000 UTC 16 September 2010 and ending 0000 UTC 18 September 2010 are examined, including a no data assimilation experiment (NODA), a cycling position and intensity-only experiment with NHC best track position and intensity assimilated at 0600, 1200, and 1800 UTC 16 September 2010 to constrain the vortex, and five cycling airborne experiments using position and intensity for the first 18 h and various

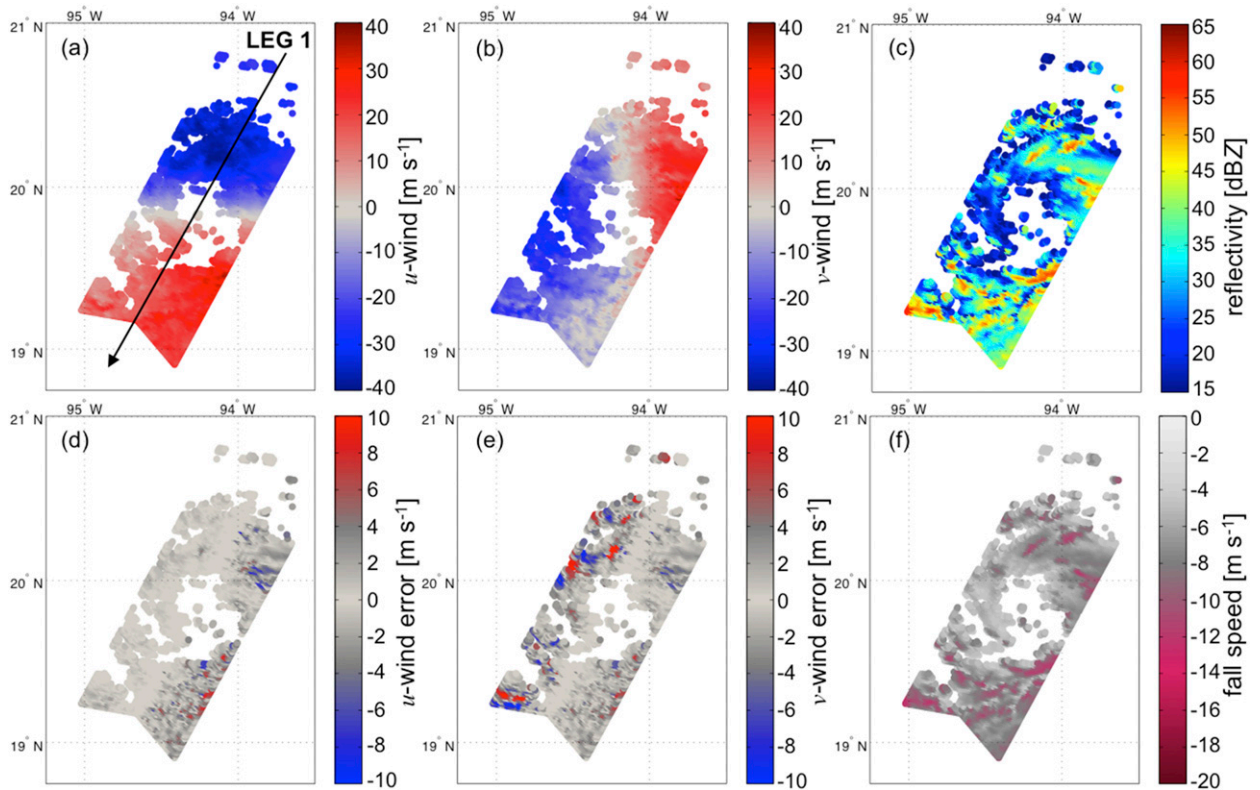


FIG. 10. WRF Model-simulated retrieved coplane observations of (a) u wind, (b) v wind, (c) maximum reflectivity, (d) u -wind error, (e) v -wind error, and (f) HRD fall speed for flight leg 1 on α plane 0° , 180° .

airborne TDR observations with a prescribed error of 3 m s^{-1} (error used for the operational radial velocity superobservations) unless otherwise stated, including coplane observations (TDRCP), coplane observations with dynamic error assignment (TDRCPU), fore/aft radial velocity observations used to generate the coplane observations (TDRVR), radial velocity superobservations, (TDRSO), and HRD observations (TDRHD).

The error used for the TDRCPU experiment incorporates the error analysis of section 4 to constrain the error based on the α -plane-dependent geometric errors inherent in the coplane methodology and raw radial velocity observations, contamination of the retrieved winds from vertically falling hydrometeors, and the temporal errors associated with the distance from the aircraft perpendicular to the aircraft track. These values are ad hoc, providing an error distribution similar to what was found in Figs. 7 and 12, minimizing closest to the aircraft with a value of 1.5 m s^{-1} and maximizing farthest from the aircraft at the largest α -plane deviation from 0° or 180° with a value of 4 m s^{-1} . All airborne data assimilation experiments use coplane observations with maximum α -plane deviation of $\pm 20^\circ$ from 0° or 180° and

within 30 km of the flight track as the errors within this data subset are similar across all methods.

For the three flight legs of the 16 September 2010 flight (Fig. 2), the simplified coplane analysis is applied, thinning the observations to the model grid resolution (3 km) valid at 1900, 2000, and 2100 UTC 16 September 2010. Using the position of the thinned coplane data, the closest HRD observation and radial velocity superobservation is found to each coplane observation along with the corresponding fore/aft radial velocity used to derive the coplane observation, thus TDRCP, TDRCPU, TDRHD, and TDRVR use the same number of observations and TDRSO uses half (only one radial velocity superobservation) to follow the real-time implementation of Weng and Zhang (2012).

Examining the forecast track, the coplane experiments (TDRCP and TDRCPU) tracks are close to the actual storm track (Fig. 13a), making landfall by 1800 UTC 17 September 2010 while the radial velocity experiments (TDRSO and TDRVR) had much slower translation and the HRD experiment (TDRHD) a more northerly track. The RMSE of the forecast track (Fig. 13c) indicates improved performance of TDRCP, TDRCPU, and TDRHD compared to direct radial

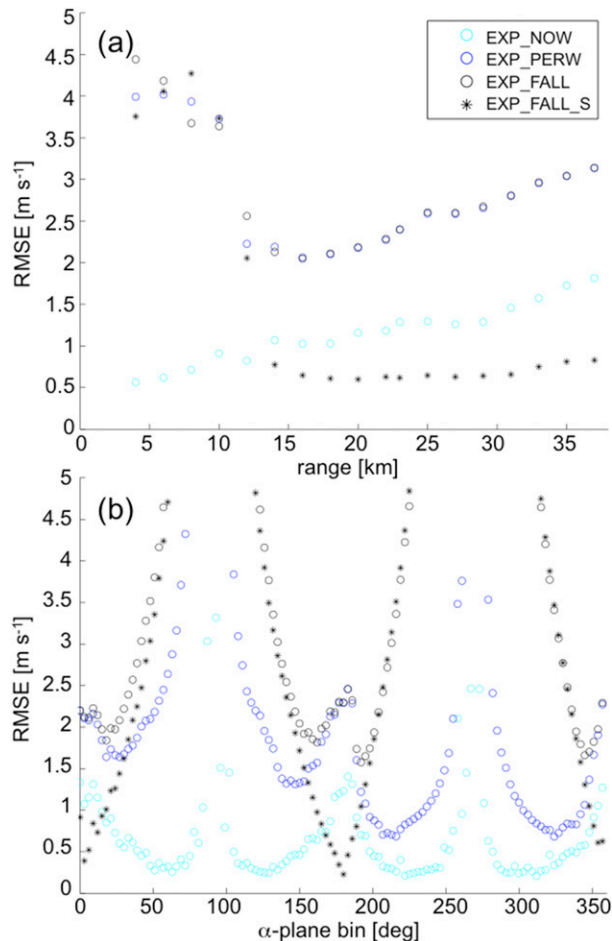


FIG. 11. Root-mean-squared error of the simulated simplified coplane analysis by (a) perpendicular distance from aircraft track and (b) α -plane bin for all simulated flight legs using no vertical component (EXP_NOW; cyan), model as the vertical component (EXP_PERW; blue), HRD terminal fall speed correction to vertical component (EXP_FALL; black), and HRD terminal fall speed correction to vertical component without temporal change in model fields (EXP_FALL_S; black asterisk) when calculating the simulated radial velocity.

velocity observations of TDRSO and TDRVR for this case.

Focusing on the maximum 10-m wind speed (Fig. 13b), all experiments underestimate the intensity at all lead times, but generally capture the strengthening of Karl as it moves into the middle of the Bay of Campeche. The TDRVR and TDRCPU forecasts provide realistic estimates of the rapid strengthening of Karl, with TDRVR having the best estimates of the intensification and weakening rates. TDRHD performs well from 21 to 27 h and at longer lead times from 36 to 45 h just before and during landfall, but weaker during the strongest stage of the storm, not capturing the rapid strengthening. At longer lead times, the TDRCP and

TDRCPU forecasts weaken more rapidly due to their faster translation, interacting with land before TDRHD, TDRSO, and TDRVR.

The analysis increment—the difference between the analysis and prior model field after the assimilation of observations—provides information about how observations and associated uncertainties in the observations and prior model field correct the prior model field. Figure 14 shows the difference in the analysis increment at a height of approximately 2250 m for the first data assimilation cycle between the TDRCPU–TDRSO and TDRCPU–TDRVR. Examining the difference in analysis increment between TDRCPU–TDRSO, the benefit of using both u and v wind at each observation point is evident, with a stronger vortex (Figs. 14a,b) and more prominent warm core (Fig. 14c) in the analysis. This same trend continued through the remaining cycles (not shown) and accounts for the weaker vortex, evident in Fig. 13b, with a much weaker TC for TDRSO. However, even though the TDRSO analysis intensity was inferior to all other airborne experiments at 2100 UTC 16 September 2010, the model dynamics were able to generate a coherent and realistic vortex over the first 6 h of the forecast and produce a competitive forecast. The inclusion of two independent fore/aft radial velocities at each observation point in TDRVR (Figs. 14d–f) substantially improves the vortex in the analysis field. The differences in analysis increments cannot be used to statistically diagnose large-scale differences between the two observation types since it is only one case, but the additional independent information provides a more representative vortex in the analysis, improved track, and improved intensity forecast compared to the operational radial velocity superobservations. The RMSE of maximum 10-m wind speed in Fig. 13c indicates that the experiments assimilating radial velocity observations reduces the intensity forecast error over experiments assimilating processed u - and v -wind components.

For this particular case, the assimilation of u - and v -wind components can improve track forecasts over radial velocities. For intensity, the experiments assimilating radial velocities provide improved 10-m wind speed forecasts with two independent radial velocity observations at each point providing the lowest error intensity forecast. It should be noted that the reduction in track and intensity forecast error between the TDRCPU and TDRCP experiments compared with the TDRHD and TDRSO experiments was not statistically significant. More systematic testing through a large number of cases, which is beyond the scope of this study, is required to more definitively evaluate the benefits of the

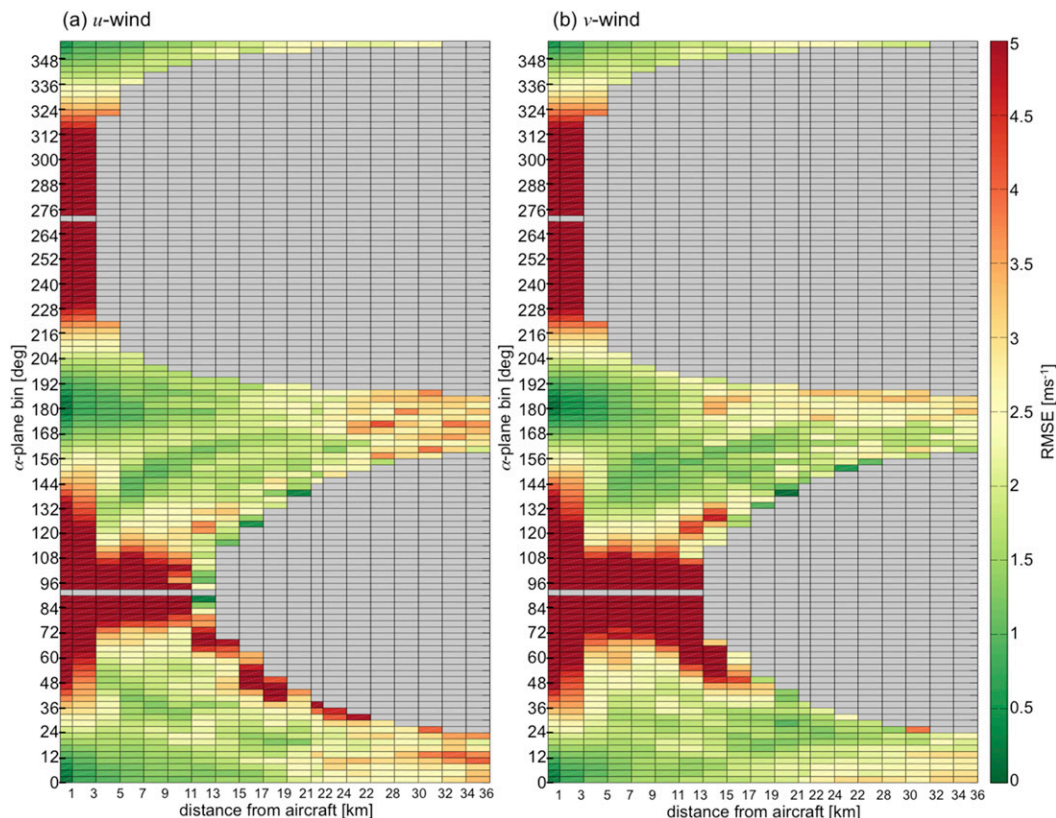


FIG. 12. Root-mean-squared error binned by α -plane bin and distance from simulated flight track for (a) u wind and (b) v wind.

simplified coplane algorithm and associated error statistics. Nevertheless, findings from the proof-of-concept experiment are in agreement with those of Li et al. (2014) who found that assimilating radial velocities enhance convective development and better resolve the inner-core structure of a TC improving the intensity forecast, while assimilating both u - and v -wind components improves the environmental flows surrounding the TC inner core, improving the track forecast.

6. Conclusions

A simplified coplane dual-Doppler technique is proposed in this study without the use of the mass continuity equation to quality-controlled airborne fore/aft radial velocities from the NOAA P3 TDR to derive low error estimate u - and v -wind components. This simplified algorithm (i) has minimal computational and I/O requirements compared to variational (HRD) or least squares minimization methods that

TABLE 3. Simulated simplified coplane analysis mean error (ME), mean absolute error (MAE), and root-mean-squared error (RMSE) of the u - and v -wind components for flight level (closest coplane observations to the simulated flight track), all coplane observations on parallel planes with the simulated aircraft wings ($\alpha = 0^\circ, 180^\circ$), coplane observations available between $\pm 50^\circ$ α -plane deviations and perpendicular distance less than 20 km from flight track, and coplane observations available between $\pm 50^\circ$ α -plane deviations at all perpendicular distances. All values are in m s^{-1} .

	u wind			v wind		
	ME	MAE	RMSE	ME	MAE	RMSE
Simulated simplified coplane analysis						
Flight level	0.00	0.08	0.21	0.01	0.08	0.02
$\alpha = 0^\circ, 180^\circ$	-0.07	1.32	2.20	0.14	1.44	2.30
$\alpha \pm 50^\circ$ distance < 20 km	-0.01	1.49	2.24	0.06	1.68	2.37
$\alpha \pm 50^\circ$	-0.03	1.59	2.40	0.08	1.69	2.42

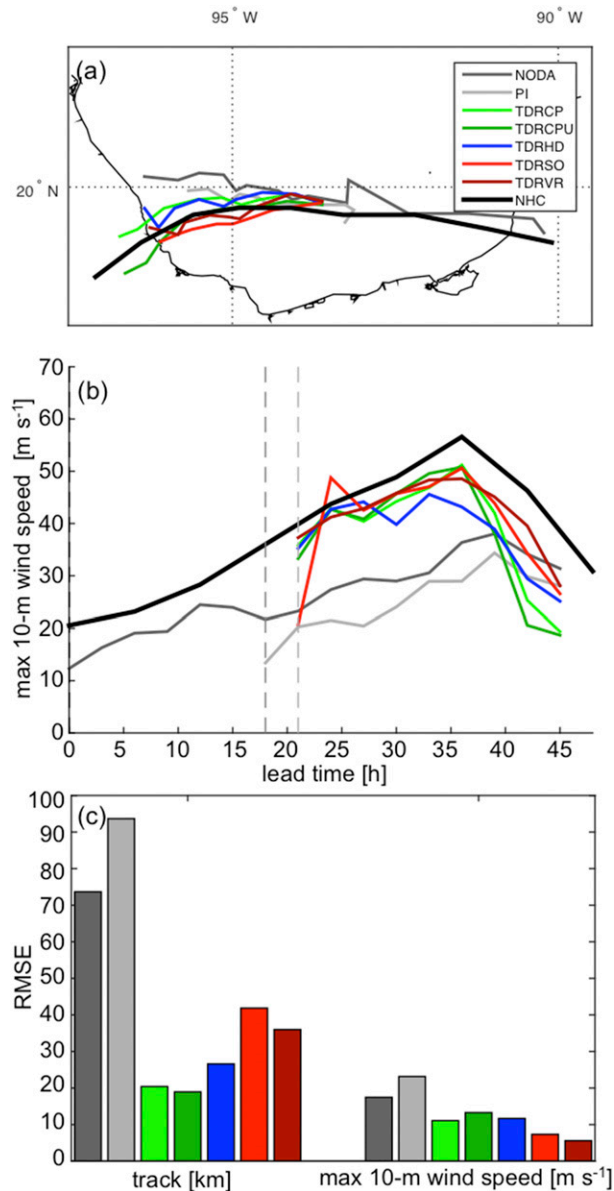


FIG. 13. PSU-WRF-EnKF data assimilation experiments forecast (a) track, (b) maximum 10-m wind speed (m s^{-1}), and (c) root-mean-squared error of track (km) and maximum 10-m wind speed (m s^{-1}) validated against the National Hurricane Center best track data from 0000 to 1800 UTC 17 Sep 2010. All experiments assimilate NHC best track and intensity for the first 18 h, except the no data assimilation experiment (NODA), and the remaining simulations assimilate airborne observations including coplane observations (TDRCP), coplane observations with error specified by distance from track and α plane (TDRCPU), HRD analysis observations (TDRHD), radial velocity superobservations (TDRSO), and raw fore/aft radial velocities used to derive the coplane observations (TDRVR). The NODA and hurricane position and minimum sea level pressure (PI) only experiments are included for reference.

have iterative solvers and increased data requirements and (ii) does not require a full flight (or multiple flight legs) to calculate retrievals, providing real-time 2D wind field retrievals. This simplified coplane algorithm provides two independent observations at a given point in space, providing two pieces of information about the wind field, estimating both along- and cross-beam wind information. The error is quantified in the retrieved along- and cross-beam winds through verification against independent in situ flight-level and dropsonde observations and through simulated observation experiments with a convection-permitting NWP model for Hurricane Karl (2010). The WRF Model simulation provides a controlled error analysis, focusing on the errors induced by the vertical fall speed correction assumption and temporal fore/aft valid time assumption. For comparison, in situ flight-level and dropsonde observations are also used to generate errors for the HRD variational analysis. The temporal errors in the coplane retrieved u - and v -wind field due to the time lag between fore/aft scans and a systematic analysis of the impact of the vertical velocity correction on the u - and v -wind field were the main focus of the study, not documented in previous literature on airborne dual-Doppler retrievals.

A superobservation procedure similar to [Weng and Zhang \(2012\)](#) is performed on the airborne Doppler radial velocity observations to bin and statistically quality control the fore/aft radial velocity observations used to derive the u - and v -wind fields. The geometry of the simplified coplane algorithm naturally thins the high spatial resolution airborne Doppler radial velocity observations.

Validating the coplane u - and v -wind observations against flight-level and dropsonde data for all pre- and postgenesis NOAA P3 flights into Hurricane Karl showed a strong dependence of error on α -plane deviation. The RMSE of the simplified coplane analysis ranges from 1.5 m s^{-1} for flight-level data closest to the aircraft track to 2.75 m s^{-1} for dropsonde validation for α -plane deviations of $\pm 50^\circ$ from the horizontal plane. The HRD variational dual-Doppler analysis showed a slightly higher RMSE error of approximately 1.75 m s^{-1} for flight-level data, hypothesized to be a consequence of the HRD analysis using mass continuity as a constraint to solve for the full three-dimensional wind field, introducing additional uncertainty. The dropsonde validation showed a lower RMSE for the u -wind retrieval, but similar v -wind retrieval ranging from approximately 2.0 to 2.5 m s^{-1} . Common in both coplane and HRD validation is the dependence of RMSE errors on the strength of the storm. The pregenesis storms generally have smaller RMSE errors than the postgenesis

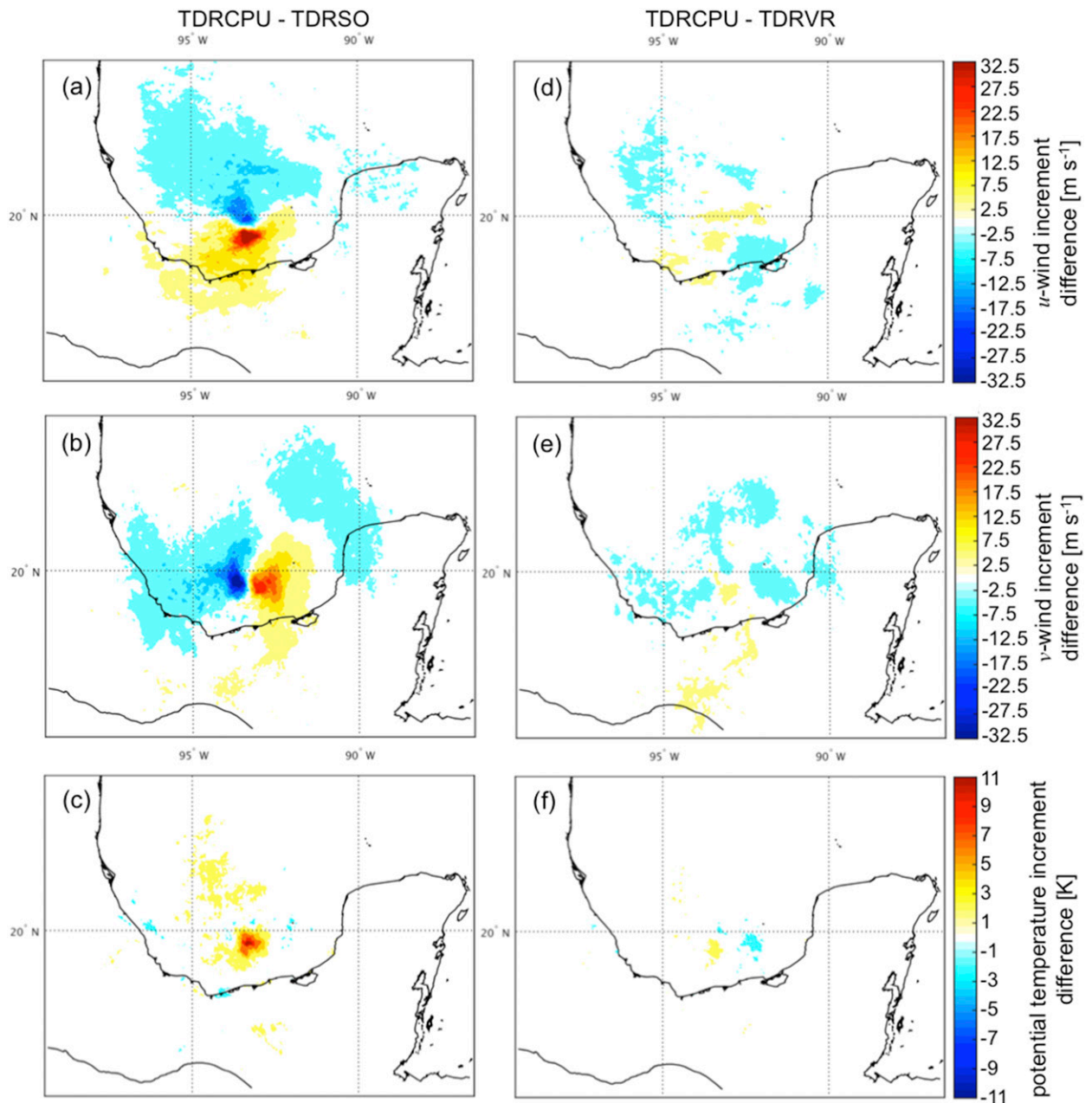


FIG. 14. Model increment (analysis minus background) difference for the first airborne TDR data assimilation cycle at 1900 UTC 16 Sep 2010 on WRF eta level 10 (~ 2250 m) for (a),(d) u wind; (b),(e) v wind; and (c),(f) potential temperature between (left) TDRCPU and TDRSO and (right) TDRCPU and TDRVR.

storms, a result of the temporal fore/aft radial assumption and wind speed magnitude.

A simulated NOAA P3 flight for the postgenesis Karl was examined to fill in gaps due to limited in situ observations. It validated the strong dependence of error on α -plane deviation and helped quantify the error in the zero vertical velocity and temporal fore/aft valid time assumptions. At perpendicular distances from the aircraft of less than 20 km, the errors are small and

generally less than 1.5 m s^{-1} . As the distance increases, the RMSE rises to $2.0\text{--}4.0 \text{ m s}^{-1}$.

The real and simulated radial velocity validation of the coplane algorithm showed that the coplane algorithm u - and v -wind components are best used within $\pm 50^\circ$ deviation in the α plane—similar to findings by Jorgensen et al. (1996)—to minimize the impact of fall speed errors and within 40 km of the aircraft to minimize temporal fore/aft errors. For purposes of assimilating

the coplane u - and v -wind observations into NWP models for TC initialization, errors should be assigned with values ranging from a minimum of approximately $1\text{--}1.5\text{ m s}^{-1}$ close to the aircraft and small α -plane deviations to approximately $4\text{--}5\text{ m s}^{-1}$ at higher α -plane deviations ($\pm 50^\circ$) and farther distance from the aircraft (40 km).

Performing a trial data assimilation experiment with the cycling PSU-WRF-EnKF for a NOAA P3 flight into Karl on 16 September showed that assimilating simplified coplane analysis observations provided similar improvements in track and intensity forecasts compared to assimilating similar HRD analysis observations, radial velocity superobservations, and both fore/aft radial velocities for a single TC case. Applying a user-specified error based on the error investigated in this improved the track, but degraded the intensity forecast when applied to the coplane observation; however, the findings were not statistically significant.

Future work is needed to further evaluate the benefits of using the simplified coplane algorithm with proper error characteristics for TC vortex initialization in NWP models. A systematic comparison of analysis and forecast errors needs to be performed for a large number of TC events over multiple cases, assimilating the simplified coplane analysis observations along with previously documented retrieval methods (e.g., Jorgensen et al. 1996; Chong and Testud 1996; Gao et al. 1999) and radial velocity superobservations. The dynamic error specification described herein should be further evaluated and additional errors included such as storm motion and beam broadening for an optimum configuration of parameters to minimize the error in TC analyses and forecasts. In addition, it would be worth exploring if an optimal combination of radial velocity and u - and v -wind components could be found that takes into account the benefit of both observations types, as Li et al. (2014) found advantage of combining both observation types in improving TC forecasts.

Acknowledgments. The authors appreciate NOAA/HRD for the real-time quality-controlled radial velocities, NOAA P3 flight-level data, and hurricane radar analysis (available online at http://www.aoml.noaa.gov/hrd/data_sub) with special thanks to John Gamache for his help with the HRD datasets and methodologies. This work has benefited from discussions with and presentations by Anthony Didlake, who implemented a dual-Doppler retrieval in cylindrical coordinates using mass continuity for the High-Altitude Imaging Wind and Rain Airborne Profiler (HIWRAP). The computing was performed at the Texas Advanced Computing Center

(TACC). This work was supported by the Office of Naval Research Grant N000140910526, the National Science Foundation Grant AGS-1305798, and NASA Grant NNX12AJ79G.

REFERENCES

- Aksoy, A., D. C. Dowell, and C. Snyder, 2010: A multicaser comparative assessment of the ensemble Kalman filter for assimilation of radar observations. Part II: Short-range ensemble forecasts. *Mon. Wea. Rev.*, **138**, 1273–1292, doi:10.1175/2009MWR3086.1.
- Armijo, L., 1969: A theory for the determination of wind and precipitation velocities with Doppler radars. *J. Atmos. Sci.*, **26**, 570–573, doi:10.1175/1520-0469(1969)026<0570:ATFTDO>2.0.CO;2.
- Atlas, D., R. C. Srivastava, and R. S. Sekhon, 1973: Doppler radar characteristics of precipitation at vertical incidence. *Rev. Geophys. Space Phys.*, **11**, 1–35, doi:10.1029/RG011i001p00001.
- Barker, D. M., W. Huang, Y.-R. Guo, A. J. Bourgeois, and Q. N. Xiao, 2004: A three-dimensional variational data assimilation system for MM5: Implementation and initial results. *Mon. Wea. Rev.*, **132**, 897–914, doi:10.1175/1520-0493(2004)132<0897:ATVDAS>2.0.CO;2.
- Bohne, A. R., and R. C. Srivastava, 1976: Random errors in wind and precipitation fall speed measurement by a triple Doppler radar system. Preprints, *17th Conf. on Radar Meteorology*, Seattle, WA, Amer. Meteor. Soc., 7–14.
- Braun, S. A., R. Kakar, E. Zipser, and G. Heymsfield, 2013: NASA's Genesis and Rapid Intensification Processes (GRIP) field experiment. *Bull. Amer. Meteor. Soc.*, **94**, 345–363, doi:10.1175/BAMS-D-11-00232.1.
- Chong, M., and C. Campos, 1996: Extended overdetermined dual-Doppler formalism in synthesizing airborne Doppler radar data. *J. Atmos. Oceanic Technol.*, **13**, 581–597, doi:10.1175/1520-0426(1996)013<0581:EODDFI>2.0.CO;2.
- , and J. Testud, 1996: Three-dimensional air circulation in a squall line from airborne dual-beam Doppler radar data: A test of coplane methodology software. *J. Atmos. Oceanic Technol.*, **13**, 36–53, doi:10.1175/1520-0426(1996)013<0036:TDACIA>2.0.CO;2.
- Didlake, A. C., G. M. Heymsfield, L. Tian, and S. R. Guimond, 2015: The coplane analysis technique for three-dimensional wind retrieval using the HIWRAP airborne Doppler radar. *J. Appl. Meteor. Climatol.*, **54**, 605–623, doi:10.1175/JAMC-D-14-0203.1.
- Frisch, A. S., L. J. Miller, and R. G. Strauch, 1974: Three-dimensional air motion measured in snow. *Geophys. Res. Lett.*, **1**, 86–89, doi:10.1029/GL001i002p00086.
- Frush, C. L., P. H. Hildebrand, and C. Walther, 1986: The NCAR airborne Doppler radar. Preprints, *23rd Conf. on Radar Meteorology*, Snowmass, CO, Amer. Meteor. Soc., 151–154.
- Gamache, J. F., 1997: Evaluation of a fully three-dimensional variational Doppler analysis technique. Preprints, *28th Conf. on Radar Meteorology*, Austin, TX, Amer. Meteor. Soc., 422–423.
- , F. D. Marks, and F. Roux, 1995: Comparison of three airborne Doppler sampling techniques with airborne in situ wind observations in Hurricane Gustav (1990). *J. Atmos. Oceanic Technol.*, **12**, 171–181, doi:10.1175/1520-0426(1995)012<0171:COTADS>2.0.CO;2.
- Gao, J., M. Xue, A. Shapiro, and K. K. Droegemeier, 1999: A variational method for the analysis of three-dimensional

- wind fields from two Doppler radars. *Mon. Wea. Rev.*, **127**, 2128–2142, doi:10.1175/1520-0493(1999)127<2128:AVMFTA>2.0.CO;2.
- Guimond, S. R., L. Tian, G. M. Heymsfield, and S. J. Frasier, 2014: Wind retrieval algorithms for the IWRAP and HIWRAP airborne Doppler radars with applications to hurricanes. *J. Atmos. Oceanic Technol.*, **31**, 1189–1215, doi:10.1175/JTECH-D-13-00140.1.
- Gunn, K. L. S., and J. S. Marshall, 1958: The distribution with size of aggregate snowflakes. *J. Meteor.*, **15**, 452–461, doi:10.1175/1520-0469(1958)015<0452:TDWSOA>2.0.CO;2.
- Hildebrand, P. H., C. Walther, and C. L. Frush, 1986: The NCAR Electra Doppler radar. Part I: Evaluation of scientific needs. Preprints, *23rd Conf. on Radar Meteorology*, Snowmass, CO, Amer. Meteor. Soc., 147–150.
- Hong, S., and J. Lim, 2006: The WRF Single-Moment 6-Class Microphysics Scheme (WSM6). *J. Korean Meteor. Soc.*, **42**, 129–151.
- , Y. Noh, and J. Dudhia, 2006: A new vertical diffusion package with an explicit treatment of entrainment processes. *Mon. Wea. Rev.*, **134**, 2318–2341, doi:10.1175/MWR3199.1.
- Iacono, M. J., J. S. Delamere, E. J. Mlawer, M. W. Shephard, S. A. Clough, and W. D. Collins, 2008: Radiative forcing by long-lived greenhouse gases: Calculations with the AER radiative transfer models. *J. Geophys. Res.*, **113**, D13103, doi:10.1029/2008JD009944.
- Jorgensen, D. P., P. H. Hildebrand, and C. L. Frush, 1983: Feasibility test of an airborne pulse-Doppler meteorological radar. *J. Climate Appl. Meteor.*, **22**, 744–757, doi:10.1175/1520-0450(1983)022<0744:FTOAAP>2.0.CO;2.
- , T. Matejka, and J. D. DuGranrut, 1996: Multi-beam techniques for deriving wind fields from airborne Doppler radars. *Meteor. Atmos. Phys.*, **59**, 83–104, doi:10.1007/BF01032002.
- Joss, J., and A. Waldvogel, 1970: Raindrop size distribution and Doppler velocities. Preprints, *14th Conf. on Radar Meteorology*, Tucson, AZ, Amer. Meteor. Soc., 153–156.
- Lee, W.-C., P. Dodge, F. D. Marks, and P. H. Hildebrand, 1994: Mapping of airborne Doppler radar data. *J. Atmos. Oceanic Technol.*, **11**, 572–578, doi:10.1175/1520-0426(1994)011<0572:MOADRD>2.0.CO;2.
- Lhermitte, R. M., and L. J. Miller, 1970: Doppler radar methodology for the observation of convective storms. Preprints, *14th Conf. on Radar Meteorology*, Tucson, AZ, Amer. Meteor. Soc., 133–144.
- Li, X., J. Ming, Y. Wang, K. Zhao, and M. Xue, 2013: Assimilation of T-TREC-retrieved wind data with WRF 3DVAR for the short-term forecasting of Typhoon Meranti (2010) near landfall. *J. Geophys. Res. Atmos.*, **118**, 10 361–10 375, doi:10.1002/jgrd.50815.
- Li, Z., Z. Pu, J. Sun, and W.-C. Lee, 2014: Impacts of 4DVAR assimilation of airborne Doppler radar observations on numerical simulations of the genesis of Typhoon Nuri (2008). *J. Appl. Meteor. Climatol.*, **53**, 2325–2343, doi:10.1175/JAMC-D-14-0046.1.
- Lorenc, A. C., 1981: A global three-dimensional multivariate statistical interpolation scheme. *Mon. Wea. Rev.*, **109**, 701–721, doi:10.1175/1520-0493(1981)109<0701:AGTDMS>2.0.CO;2.
- Lorsolo, S., J. Gamache, and A. Aksoy, 2013: Evaluation of the Hurricane Research Division Doppler radar analysis software using synthetic data. *J. Atmos. Oceanic Technol.*, **30**, 1055–1071, doi:10.1175/JTECH-D-12-00161.1.
- Marks, F. D., and R. A. Houze, 1984: Airborne Doppler radar observations in Hurricane Debby. *Bull. Amer. Meteor. Soc.*, **65**, 569–582, doi:10.1175/1520-0477(1984)065<0569:ADROIH>2.0.CO;2.
- , and —, 1987: Inner core structure of Hurricane Alicia from airborne Doppler radar observations. *J. Atmos. Sci.*, **44**, 1296–1317, doi:10.1175/1520-0469(1987)044<1296:ICSOHA>2.0.CO;2.
- Mohr, C. G., L. J. Miller, and R. L. Vaughan, 1981: An interactive software package for the rectification of radar data to three-dimensional Cartesian coordinates. Preprints, *20th Conf. on Radar Meteorology*, Boston, MA, Amer. Meteor. Soc., 690–695.
- Montgomery, M. T., C. Davis, T. Dunkerton, Z. Wang, and C. Velden, 2012: The Pre-Depression Investigation of Cloud-Systems in the Tropics (PREDICT) experiment: Scientific basis, new analysis tools, and some first results. *Bull. Amer. Meteor. Soc.*, **93**, 153–172, doi:10.1175/BAMS-D-11-00046.1.
- Poterjov, J., and F. Zhang, 2011: Dynamics and structure of forecast error covariance in the core of a developing hurricane. *J. Atmos. Sci.*, **68**, 1586–1606, doi:10.1175/2011JAS3681.1.
- Purser, R. J., D. F. Parrish, and M. Masutani, 2000: Meteorological observational data compression; An alternative to conventional “super-Obbing.” Office Note 430, National Centers for Environmental Prediction, Camp Springs, MD, 12 pp.
- Ray, P. S., R. J. Doviak, G. B. Walker, D. Sirmans, J. Carter, and B. Bumgarner, 1975: Dual-Doppler observation of a tornadic storm. *J. Appl. Meteor.*, **14**, 1521–1530, doi:10.1175/1520-0450(1975)014<1521:DDOAT>2.0.CO;2.
- , C. L. Ziegler, W. Bumgarner, and R. J. Serafin, 1980: Single-and multiple-Doppler radar observations of tornadic storms. *Mon. Wea. Rev.*, **108**, 1607–1625, doi:10.1175/1520-0493(1980)108<1607:SAMDRO>2.0.CO;2.
- Reasor, P. D., M. D. Eastin, and J. F. Gamache, 2009: Rapidly intensifying Hurricane Guillermo (1997). Part I: Low-wavenumber structure and evolution. *Mon. Wea. Rev.*, **137**, 603–631, doi:10.1175/2008MWR2487.1.
- Rogers, R. R., 1964: An extension of the ZR relation for Doppler radar. Preprints, *11th Conf. on Radar Meteorology*, Boulder, CO, Amer. Meteor. Soc., 158–161.
- Rogers, R., and Coauthors, 2006: The Intensity Forecasting Experiment: A NOAA multiyear field program for improving tropical cyclone intensity forecasts. *Bull. Amer. Meteor. Soc.*, **87**, 1523–1537, doi:10.1175/BAMS-87-11-1523.
- Skamarock, W. C., and Coauthors, 2008: A description of the Advanced Research WRF version 3. NCAR Tech Note NCAR/TN-475+STR, 113 pp., doi:10.5065/D68S4MVH.
- Stoelinga, M. T., 2005: Simulated equivalent reflectivity factor as currently formulated in RIP: Description and possible improvements. Read/Interpolate/Plot Implementation Document, 5 pp. [Available online at <http://citeserx.ist.psu.edu/viewdoc/download?doi=10.1.1.522.925&rep=rep1&type=pdf>].
- Wang, M., M. Xue, K. Zhao, and J. Dong, 2014: Assimilation of T-TREC-retrieved winds from single-Doppler radar with an ensemble Kalman filter for the forecast of Typhoon Jangmi (2008). *Mon. Wea. Rev.*, **142**, 1892–1907, doi:10.1175/MWR-D-13-00387.1.
- Weng, Y., and F. Zhang, 2012: Assimilating airborne Doppler radar observations with an ensemble Kalman filter for convection-permitting hurricane initialization and prediction: Katrina (2005). *Mon. Wea. Rev.*, **140**, 841–859, doi:10.1175/2011MWR3602.1.
- Zhang, C., Y. Wang, and K. Hamilton, 2011: Improved representation of boundary layer clouds over the southeast Pacific in

- ARW-WRF using a modified Tiedtke cumulus parameterization scheme. *Mon. Wea. Rev.*, **139**, 3489–3513, doi:[10.1175/MWR-D-10-05091.1](https://doi.org/10.1175/MWR-D-10-05091.1).
- Zhang, F., and Y. Weng, 2015: Predicting hurricane intensity and associated hazards: A five-year real-time forecast experiment with assimilation of airborne Doppler radar observations. *Bull. Amer. Meteor. Soc.*, **96**, 25–33, doi:[10.1175/BAMS-D-13-00231.1](https://doi.org/10.1175/BAMS-D-13-00231.1).
- , —, J. A. Sippel, Z. Meng, and C. H. Bishop, 2009: Cloud-resolving hurricane initialization and prediction through assimilation of Doppler radar observations with an ensemble Kalman filter. *Mon. Wea. Rev.*, **137**, 2105–2125, doi:[10.1175/2009MWR2645.1](https://doi.org/10.1175/2009MWR2645.1).
- , —, J. F. Gamache, and F. D. Marks, 2011: Performance of convection-permitting hurricane initialization and prediction during 2008–2010 with ensemble data assimilation of inner-core airborne Doppler radar observations. *Geophys. Res. Lett.*, **38**, L15810, doi:[10.1029/2011GL048469](https://doi.org/10.1029/2011GL048469).
- Ziegler, C. L., 1978: A dual Doppler variational objective analysis as applied to studies of convective storms. M.S. thesis, University of Oklahoma, 115 pp.